# Differential Reactivation of Task-Demand-Associated Firing Patterns in Subicular and CA1 Place Cells during a Hippocampal Memory Task

Jae-Min Seol†, Su-Min Lee† and Inah Lee*

Department of Brain and Cognitive Sciences
Seoul National University
Gwanak-ro 1, Gwanak-gu
Seoul 08826, South Korea

†These authors contributed equally
*Corresponding author
E-mail: inahlee@snu.ac.kr
Phone: +82-2-880-8013

## Acknowledgments

This research was supported by National Research Foundation of Korea Grants 2019R1A2C2088799, 2021R1A4A2001803, 2022M3E5E8017723, and 2022R1I1A1A01069756.

**Abstract**

Reactivation of place cells during sharp-wave ripples (SWRs) in the hippocampus is pivotal for memory consolidation, yet the SWR dynamics between the hippocampus and its neighboring subiculum remain underexplored. This study examined the differential SWR-associated reactivations of task-demand-associated representations in the subiculum and CA1 during a visual scene memory task in rats. In the task, the spiking activities of place-cell ensembles were reactivated during a SWR event according to task demands. These reactivations were more frequent and associated with more heterogeneous task-demand types in the subiculum compared to CA1. These subicular characteristics were driven by multiple subfields within the subicular place field, parcellated by the theta phase precession cycle. In contrast, CA1 exhibited a higher incidence of spatial replay than the subiculum. These findings indicate that the subiculum plays a key role in transmitting task-specific variables from the hippocampus to other brain regions.

**Teaser**

The subiculum more frequently and dynamically reactivates the neural representations linked to task demands than the hippocampal CA1.

## Introduction

Episodic memory involves the recollection of events within a spatial context. Such memories comprise not only the locations where events occurred but also encompass other related elements such as objects and background contexts. It has been widely postulated that the hippocampus is vital for both the formation and retrieval of these event memories (*1,2*). Additionally, research indicates that the consolidation of event memory requires specific physiological mechanisms in the hippocampus, particularly sharp wave ripples (SWRs), which are believed to play a crucial role during the process of memory consolidation in learning (3-5).

Literature suggests that SWRs facilitate the reinstatement of spatial information in the hippocampus by the 'replay' of place cells according to their spatial firing patterns observed during prior exploration (*6-8*). Numerous studies have demonstrated that task-related information can influence these replay patterns. For instance, the amount of reward (*9-11*) or the valence associated with a location (*12-14*) modulates neural activity during SWRs by affecting the participation rates of certain cell types or directing robust replays toward significant locations. Moreover, replayed sequences are responsive to obstacles or shortcuts (*15,16*), and place cells' firing rates are adjusted based on contextual differences (*17-19*). These findings indicate that task-relevant factors influence the spatial reactivation patterns of place cells. However, there is limited understanding of whether the spiking activities of place cells, whose firing patterns are modulated by such task-relevant information, are reinstated more often during SWRs merely in quantity, irrespective of the replay of place cells.

With respect to the areas in which SWR-dependent reactivations occur, it is well-established that hippocampal reactivation of neural activities is a robust phenomenon and is critical for learning and memory (*4,5,20-25*). However, the role of its cortical output interface, the subiculum, in this process remains largely unexplored. The subiculum has been proposed as a crucial pathway for transmitting hippocampal activities, including SWRs, to neocortical areas (*26*), or as a region capable of generating SWRs independently (*27*). It has also been reported that a subset of subicular neurons either increase or decrease their firing rates during SWRs (*28,29*). Nonetheless, it is unclear whether subicular neurons are reactivated in relation to the spatial and non-spatial information of event memory during

SWRs, especially considering their broader spatially tuned firing patterns compared to CA1 place cells (*30-34*). The differences between the CA1 and subiculum suggests potential variations in reactivation patterns between the hippocampus and subiculum after experiencing an event.

Our previous research (*32,34*) identified distinct firing properties of subicular neurons related to task-relevant information in a hippocampal memory task. Specifically, in a visual scene memory (VSM) task, place cells in both the subiculum and CA1 demonstrated firing-rate modulations (rate remapping) based on the visual scenes in the background or the impending arm choice. These rate-remapping events were observed in a θ-phase-based subfield defined by the θ-phase precession phases of spikes. Additionally, the θ-phase-based subfields of subicular neurons showed stronger modulation of firing rates in response to critical task variables (i.e., visual scenes and associated choice arms), termed 'TDA (task-demand-associated) variables' in this study. Building on our previous findings, we hypothesize that subicular neuronal ensembles coactivated during SWRs may represent TDA information more prominently than hippocampal ensembles.

## Results

### Behavioral Performance in a Hippocampal-Dependent Visual Scene Memory Task

The data utilized in this study were originally collected in our previous research (*32*). Five rats were trained to associate four distinct visual scene stimuli with either the left or right arm of a T-maze as part of a visual scene memory (VSM) task (**Figure 1**). During each trial, the rat would start from the start box at one end of the stem and move toward the intersection at the opposite end. At the beginning of each trial, the guillotine door of the start box was opened, allowing the rat to walk onto the maze stem, while one of the four visual scenes (pseudo-randomly selected for each trial) was displayed on an array of three LCD monitors surrounding the choice area of the maze. The rat needed to visit the arm associated with the presented scene stimulus to retrieve a cereal reward from the food well. After making a choice and returning to the start box with the cereal reward to consume it, the guillotine door was closed, signaling the start of the inter-trial interval (ITI). Our previous research indicated that the VSM task is dependent on the hippocampus (*35*) as well as the subiculum (*36*).

By the time the physiological recording sessions began, all rats had surpassed the performance criterion (75% correct choices) for all scene stimuli ($Z = 3.94$, $p < 0.001$ for zebra; $Z = 3.91$, $p < 0.001$ for pebbles; $Z = 3.75$, $p < 0.001$ for bamboo; $Z = 3.91$, $p < 0.001$ for mountain; one-sample Wilcoxon signed rank test). There was no significant difference in the ITIs across the different scene conditions ($F_{(3)} = 0.14$, $p = 0.936$, one-way ANOVA; **Figure S1**). We simultaneously recorded spiking activities from single units and local field potentials (LFPs) from the dorsal CA1 and subiculum while the rats performed the VSM task. Consistent with our previous findings (*32,34*), the average firing rate of complex-spiking cells (n = 192 in the subiculum; n = 282 in the CA1) was higher in the subiculum than in the CA1 ($Z = 8.45$, $p < 0.001$), while the spatial information score (bit/spike) was lower in the subiculum compared to the CA1 ($Z = -12.51$, $p < 0.001$; Wilcoxon rank-sum test).

SWRs were defined as LFP signals with high frequency (150-250 Hz) and large amplitude (> 2 standard deviations, or SDs, for the SWR peak, and > 0.5 SD for its boundaries; see Material and Methods for details) (**Figure 1**). SWRs analyzed in this study occurred during ITIs following correct trials when the rats were awake but immobile. We included a SWR event in further analysis only if three or more putative complex-spiking cells fired simultaneously (n = 5899 in the subiculum; n = 1899 in the CA1) (**Figure 1**). SWRs in the subiculum were shorter in duration ($Z = -3.11$, $p = 0.002$; **Figure S2**) and involved fewer coactivated cells per SWR ($Z = -33.47$, $p < 0.001$) compared to CA1 SWRs. Additionally, the amplitude of the filtered LFP was larger in the subiculum compared to the CA1 ($Z = 31.74$, $p < 0.001$; Wilcoxon rank-sum test).

## Selective Firing of Subiculum and CA1 Place Cells for Visual Scene Stimuli and Upcoming Choices

In our previous study (*34*), we demonstrated that the traditional spatial firing field (place field), defined by the firing rate ('rate-based field'), could be further subdivided into multiple subfields ('θ-phase-based fields') based on the cell's theta phase precession cycle. This method revealed spatially localized subfields within the broad firing field of a subicular neuron, making the subicular θ-phase-based fields comparable to the rate-based fields in CA1 in most firing properties. We applied the same θ-phase-based field identification method in

the current study to define θ-phase-based place fields in both the subiculum and CA1 (**Figure 2A**).

Among the cells exhibiting at least one θ-phase-based field (n = 135 in the subiculum; n = 168 in CA1), single place fields (SF cells) were more prevalent in CA1 (74.4%) compared to the subiculum (31.1%), whereas multiple place fields (MF cells) were more common in the subiculum (68.9%) than in CA1 (25.6%) ($\chi^2_{(2)} = 196.84$, $p < 0.001$; chi-squared test) (**Figure 2B**). Notably, a significant proportion of subicular MF cells had more than two subfields, while most CA1 MF cells typically exhibited only two subfields. The average firing rates of individual subfields were higher in SF cells than in MF cells in both regions (**Figure 2C**). A two-way ANOVA with the number of fields and region as factors revealed a significant effect of the number of fields on average firing rates ($F_{(1,493)} = 37.45$, $p < 0.001$) but not for the region ($F_{(1,493)} = 2.31$, $p = 0.13$). Post-hoc comparison showed that the average firing rates of individual fields of SF cells were significantly higher than those of MF cells in both regions ($t_{(272)} = 3.69$, $p < 0.001$ in the subiculum; $t_{(218)} = 5.42$, $p < 0.001$ in CA1). When the number of fields was matched, there was no significant difference in average firing rates between the subiculum and CA1 ($t_{(165)} = 0.75$, $p = 0.454$ for SF cells; $t_{(325)} = 1.573$, $p = 0.117$ for MF cells). The field width differed significantly between SF and MF cell types ($F_{(1,493)} = 35.65$, $p < 0.001$), especially in the subiculum ($t_{(272)} = 5.63$, $p < 0.001$) but less so in CA1 ($t_{(218)} = 1.96$, $p = 0.051$) (**Figure 2D**). As previously reported, subicular cells had larger place fields than CA1 cells ($F_{(1,493)} = 35.65$, $p < 0.001$), even when the number of fields was matched ($t_{(165)} = 6.99$, $p < 0.001$ for SF cells; $t_{(325)} = 3.72$, $p < 0.001$ for MF cells; Bonferroni-corrected two-sample t-test).

The θ-phase-based field identification method enabled us to identify task-demand-associated (TDA) rate modulation in the subiculum and CA1 (*34*) (**Figure 2A**). In the VSM task, visual scenes and upcoming choice arms were defined as TDA variables. We quantified the strength of rate modulation for each θ-phase-based place field using the scene selectivity index (SSI) for visual scene pairs associated to the same rewarding arm: $SSI_L$ for the zebra-bamboo pair and $SSI_R$ for the pebbles-mountain pair. Additionally, we calculated a choice selectivity index (CSI) to measure rate modulation strength based on the upcoming arm choice (see Material and Methods for details). A positive selectivity index indicated selective firing for the zebra scene, pebbles scene, or left-arm choice, whereas a negative index

indicated selective firing for the bamboo scene, mountain scene, or right-arm choice. When we compared the distribution of the selectivity indices of all θ-phase-based place fields, similar levels of selectivity were observed between the subiculum and CA1 for all three task demands ($p = 0.633$ for $SSI_L$; $p = 0.199$ for $SSI_R$; $p = 0.642$ for CSI; Kolmogorov-Smirnov test; **Figure S3A**).

We assessed the extent of rate modulation by comparing the absolute values of selectivity indices measuring the scene- and choice-associated task demands (**Figure S3B**). A two-way ANOVA showed significant differences between SF and MF cells for all three types of task demands ($F_{(1, 299)} = 5.84$, $p < 0.001$ for $SSI_L$; $F_{(1, 298)} = 4.53$, $p < 0.001$ for $SSI_R$, $F_{(1,292)} = 1.98$, $p = 0.049$ for CSI), while subiculum and CA1 differences were insignificant ($F_{(1, 299)} = 1$, $p = 0.32$ for $SSI_L$; $F_{(1, 298)} = 0.15$, $p = 0.88$ for $SSI_R$, $F_{(1,292)} = 0.53$, $p = 0.6$ for CSI). Specifically, $SSI_L$ and $SSI_R$ were larger in MF cells than in SF cells in both regions ($t_{(133)} = -5.06$, $p < 0.001$ in subiculum, $t_{(166)} = -3.3$, $p = 0.001$ in CA1 for $SSI_L$; $t_{(133)} = -3$, $p = 0.003$ in subiculum, $t_{(165)} = -3.42$, $p < 0.001$ in CA1 for $SSI_R$). However, CSI was not significantly higher in MF cells than in SF cells in both regions ($t_{(132)} = -1.81$, $p = 0.073$ in subiculum, $t_{(160)} = -0.9$, $p = 0.369$ in CA1; Bonferroni-corrected two-sample t-test).

In summary, the overall neural firing characteristics were consistent between the subiculum and CA1 despite some differences between SF and MF cells. Importantly, our results demonstrated that cells in the subiculum and CA1 represented TDA variables (i.e., visual scenes and upcoming choice arms) through rate modulation at the level of θ-phase-based fields in the VSM task.

## Enhanced Reactivation of TDA Cells During Awake SWRs in the Subiculum Compared to CA1

Upon validating that place cells in the subiculum and CA1 exhibit rate modulation in response to task demands, we investigated whether the ensemble of cells reactivated simultaneously within an awake SWR event showed bias toward specific task conditions, such as a particular visual scene stimulus or choice arm. If most cells in a SWR-reactivated ensemble exhibited higher activities for a common task variable, we considered the ensemble to be reactivated for that task variable during the SWR event. We termed the reactivation of cells exhibiting significant correlations with task demands as 'TDA reactivation.'

We defined TDA reactivation with the following criteria. First, the cell ensemble needed to be identifiable within the SWR boundaries. Then, we parsed the overall firing rate maps of the cells into individual subfields to measure the selectivity indices of individual θ-phase-based fields (**Figure 3**). Fields with low selectivity indices (between -0.1 and 0.1) were excluded from the analysis. Cells with low selectivity indices for all subfields were further excluded from the analysis (1 subicular cell and 5 CA1 cells). Subsequently, these field-based firing rate maps were reconstructed for various task demands (i.e., zebra vs. bamboo scene, pebbles vs. mountain scene, left vs. right choice arm) (**Figure 4**).

To quantify TDA rate modulation at the ensemble level, a cell's representative selectivity index for each task demand was calculated by finding the maximum value of the absolute selectivity indices among all task-demand-selective subfields of the cell (yellow or blue bars in **Figure 4A-C**). For example, the subicular SWR event illustrated in **Figure 4** includes the reactivation of an ensemble whose scene-selective fields exhibited higher firing rates for the pebbles scene compared to the mountain scene. The bias toward the pebbles scene was also verified by the distribution of selectivity indices (**Figure 4B**), with all cells' representative selective indices showing positive values (yellow bars).

Our results revealed that a significant proportion of SWRs in both regions contained cell ensembles demonstrating substantial TDA reactivations for specific scenes or arm choices (**Figure 5A** and **Figure S4**). Notably, a significantly larger proportion of SWRs in the subiculum (61.5%) exhibited TDA reactivation compared to the CA1 (41.5%) ($\chi^2_{(1)} = 170.9$, $p < 0.001$; chi-squared test) (**Figure 5B**). Additionally, the p-values from the binomial tests were significantly lower in the subiculum compared to CA1 across all three task demands ($Z = -12.57$, $p < 0.001$ for $SSI_L$, $Z = -5.81$, $p < 0.001$ for $SSI_R$, $Z = -7.48$, $p < 0.001$ for CSI; Wilcoxon rank-sum test) (**Figure 5C**), indicating a higher tendency for co-activation of cells encoding identical task demands during SWRs in the subiculum than in CA1.

Our findings demonstrate that cell assemblies representing crucial TDA variables, such as visual scenes and upcoming arm choices, are reactivated during an SWR event. More importantly, TDA neural reactivation is more prevalent and robust in the subiculum than in CA1.

227 **Simultaneous Representation of Diverse Task Demands During TDA Neural**
228 **Reactivation**

229 Cells in the subiculum have demonstrated a superior ability to represent multiple TDA
230 variables, such as scene and arm choice, in the VSM task compared to those in the CA1
231 region (*34*). In the present study, we further investigated whether different task demands were
232 simultaneously represented by cell ensembles during SWR events. **Figure 6A** exemplifies
233 SWR events wherein a scene or choice variable (or both) was represented during neural
234 reactivations. Most SWRs exhibiting significant TDA reactivations showed scene selectivity
235 only (68.4% in the subiculum; 65.6% in CA1), while others demonstrated choice-arm-
236 selective reactivations exclusively (13% in the subiculum; 19.6% in CA1) (**Figure 6B**).
237 Notably, a subset of SWRs reactivated cell ensembles representing both visual scene and
238 choice-arm variables simultaneously, and these were more prevalent in the subiculum
239 (18.5%) compared to CA1 (14.7%) ($\chi^2_{(1)} = 5.8$, $p = 0.016$; chi-squared test).

240 Our findings indicate that neural ensembles reactivated during SWR events do not
241 simply represent a single type of task demand; rather, they often encode multiple types of
242 TDA variables (i.e., visual scenes and upcoming choice arms) within the same SWR event.
243 Furthermore, reactivations encompassing heterogeneous task demands occurred more
244 frequently in SWRs recorded from the subiculum than from CA1. These results support our
245 previous findings that subicular MF cells represent diverse task demands through their
246 multiple θ-phase-based subfields (*34*).

247

248 **Theta-Phase-Based Multi-Field Cells Drive TDA Reactivation in the Subiculum**

249 Considering the superior ability of subicular MF cells to process heterogeneous TDA
250 variables, such as visual scene and choice-arm information, in comparison to CA1 MF cells
251 (*34*), we theorized that the increased frequency and diversity of TDA reactivations in the
252 subiculum might be linked to the higher presence of MF cells in this area relative to CA1.

253 Our observations revealed that heightened neural activity in certain subicular MF
254 cells coincided with TDA reactivations during SWR events (**Figure 7A**). Conversely, the
255 activities of subicular SF cells remained relatively stable, irrespective of the presence of TDA
256 reactivations during SWRs. In contrast, SF cells in CA1 showed an increase in firing rates

during SWRs while exhibiting TDA reactivations, unlike their MF counterparts. This observation was further supported by a larger proportion of subicular MF cells within a reactivated ensemble during SWR events, particularly when TDA reactivations were present ($Z = -15.05$, $p < 0.001$) (**Figure 7B**). However, a similar trend was not observed in CA1 ($Z = 0.26$, $p = 0.8$; Wilcoxon rank-sum test).

To mitigate the potential influence of varying MF cell numbers between the regions, we analyzed the participation rates of each cell type in SWR events. Subicular MF cells displayed higher engagement in SWRs with TDA reactivations compared to those without such reactivations ($t_{(176)} = 9.12$, $p < 0.001$). In contrast, subicular SF cells did not exhibit such differential behavior ($t_{(72)} = 0.08$, $p = 0.93$) (**Figure 7C**). Both MF and SF cell types in CA1 demonstrated a marked increase in participation rates in SWRs with TDA reactivations ($t_{(81)} = 3.28$, $p = 0.002$ for MF cells; $t_{(247)} = 5.68$, $p < 0.001$ for SF cells). Comparing participation rates in SWRs with TDA reactivations, subicular MF cells exhibited significantly higher rates compared to SF cells ($t_{(115)} = -4.88$, $p < 0.001$). Conversely, the difference in SWR participation rates between MF and SF cells in CA1 was not significant ($t_{(162)} = 0.36$, $p = 0.72$). For TDA reactivations in the absence of SWRs, the participation rate difference between MF and SF cells was insignificant in both the subiculum and CA1 ($t_{(133)} = -0.66$, $p = 0.51$ in the subiculum; $t_{(166)} = 0.09$, $p = 0.93$ in CA1; Bonferroni-corrected two-sample t-test).

Moreover, the SWR-based TDA reactivations significantly decreased when the analysis was conducted using place fields defined by firing rates, particularly in the subiculum where most cells exhibited broad single fields ($\chi^2_{(1)} = 23.7$, $p < 0.001$; chi-squared test for proportions of TDA reactivation in the subiculum and CA1) (**Figure S5**).

Our results indicate that subicular cells with multiple θ-phase-based subfields may be pivotal in driving the frequent and robust reactivation of TDA variables during SWRs.

## More Prevalent Spatial Reactivations during SWRs in CA1 than in Subiculum

We investigated whether spatial reactivation (i.e. spatial replay of place fields) (*6-8*) was also found during the awake SWR events in both regions in our study. To analyze spatial reactivation, we utilized the complete on-track firing patterns of cells instead of θ-phase-based fields due to the challenge of assigning spikes during SWR events to specific fields.

Bayesian decoding was implemented to calculate the posterior probability of locations on the maze, generating a linear regression strength value ($R^2$) (**Figure S6**; for detailed methodology, refer to Material and Methods).

Our observations revealed similar patterns of spatial reactivations in both the subiculum and CA1 regions (**Figure 8A**). Interestingly, the percentage of SWRs exhibiting spatial reactivation was significantly higher in CA1 (20.0%) compared to the subiculum (6.0%) ($\chi^2_{(1)} = 729.04$, $p < 0.001$; chi-squared test) (**Figure 8B**). Moreover, the linear regression strength was notably greater in CA1 than in the subiculum ($Z = -19.81$, $p < 0.001$; Wilcoxon rank-sum test) (**Figure 8C**). Notably, only a small fraction of SWRs in CA1 (3.4%) and the subiculum (1.2%) demonstrated both spatial and TDA reactivations, suggesting the separate occurrence of these two types of reactivations in most instances.

Furthermore, the presence of spatial reactivations led to a decrease in the proportion of subicular MF cells within the reactivated ensemble, unlike in CA1 ($t_{(5897)} = 21.47$, $p < 0.001$ in the subiculum; $t_{(1889)} = 0.54$, $p = 0.59$ in CA1; two-sample t-test) (**Figure 8D**). This decline in the proportion of MF cells during spatial reactivations supports the independent nature of spatial and TDA reactivations, aligning with prior studies highlighting the pivotal role of subicular MF cells in TDA reactivations.

These findings indicate that while spatial reactivation, often referred to as "replay", occurs in subicular SWRs, its frequency and robustness are lower compared to CA1.

## Discussion

In our current investigation, we differentiated the SWR-associated firing patterns of neurons in the subiculum from those in the CA1 region of the hippocampus using the θ-phase-based field parcellation method. Notably, we found that the reactivation of TDA variables during SWRs was more pronounced in the subiculum than in the CA1. Additionally, there was a higher incidence of SWRs representing diverse TDA variables in the subiculum compared to CA1. Specifically, subicular neurons with multiple θ-phase-based fields demonstrated increased involvement in TDA reactivation. Interestingly, while spatial replays were also identified in the subiculum, they occurred at a lower frequency than in the hippocampus.

Crucially, these spatial replays in the subiculum were observed independently of TDA reactivations. Collectively, our results highlight the pivotal role of the subiculum in facilitating the transmission of crucial task-relevant information between the hippocampus and cortical regions during hippocampal memory tasks.

**Multiple θ-Phase-Based Place Fields Drive Frequent and Diverse TDA Reactivations in the Subiculum**

Several studies have demonstrated a correlation between neural activities in the subiculum and hippocampal SWRs (*28,29*). Bohm et al. (2015) found that subicular neurons exhibited varying responses to hippocampal SWRs based on their intrinsic firing patterns. They utilized whole-cell current-clamp recordings in both awake, head-fixed mice and in vitro settings to classify subicular pyramidal cells as either bursting or regular spiking. Around the peak of the ripple, the firing rates of bursting cells increased, whereas those of regular spiking cells decreased. Similarly, Kitanishi et al. (2021) observed ripple-associated firing rate modulation in subicular excitatory neurons, noting the modulation varied depending on the efferent regions to which the neurons projected. Specifically, neurons projecting to the anteroventral thalamus were suppressed, whereas those projecting to the nucleus accumbens or medial mammillary body were activated following hippocampal SWRs. These findings indicate that subicular neurons are responsive to hippocampal SWRs, although the specific type of information represented during these events in the subiculum remains unclear.

In this study, we examined the reactivation of task-demand-associated information during SWRs in the subiculum. We utilized data from our previous study (*34*) to determine the type and extent of information represented by subicular compared to hippocampal neurons in the VSM task. Notably, we developed a novel method to define subicular place fields based on spiking phases relative to local theta oscillations. We found that two-thirds of the recorded cells were classified as having multiple θ-phase-based place fields (MF) in the subiculum, displaying firing properties similar to typical place fields in the CA1. These MF cells exhibited greater selectivity for task variables than SF cells in the subiculum and encoded heterogeneous TDA variables through their multiple subfields.

We hypothesized that subicular MF cells play a critical role in hippocampal-

347 dependent associative memory tasks. Supporting our hypothesis, the unique firing
348 characteristics of subicular MF cells significantly influenced TDA reactivations during
349 SWRs. Specifically, subicular MF cells selectively increased their participation rates in
350 SWRs when TDA information was reactivated (**Figure 7C**), leading to the reactivation of
351 heterogeneous task-related information within a single SWR event (**Figure 6**). These results
352 not only confirm our previous findings but also suggest a functional diversity of subicular
353 principal neurons in episodic memory.

354 We further observed that the participation rates of SF cells and MF cells in TDA
355 reactivations varied only in the subiculum, even though the overall firing profiles of MF cells
356 on the track were similar between the subiculum and CA1 (**Figure 2**). The selective
357 involvement of subicular MF cells in TDA reactivations might be due to their orthogonal
358 representations (*34*). This means that the task-relevant variables showing the greatest
359 selectivity differed across multiple fields of a single neuron. For example, one field might
360 represent a visual scene, while another field represents an upcoming choice arm. In contrast,
361 in most cases of CA1 MF cells, heterogeneous representations were driven by individual
362 single fields. This suggests that SF cells and MF cells in the CA1 do not functionally differ in
363 representing TDA variables, which explains why the participation rates in TDA reactivation
364 were similar between the two cell types in the CA1.

365 To examine TDA reactivations, the subfield with the highest selectivity index among
366 multiple fields was chosen as the representative field for each TDA variable. A limitation of
367 this analysis is that it is difficult to assume that a spike generated during SWR originates from
368 a specific field. The current analysis assumed that the spike signals the TDA variable with the
369 highest selectivity index, which is most strongly represented by the cell. This issue also arises
370 in spatial reactivation analysis for place cells with multiple place fields. Particularly in large
371 spaces or environments with many repetitive compartments, a significant portion of place
372 cells exhibited multiple place fields in the hippocampus (*37-40*). A method that determines
373 which specific field or information a spike represents during SWR signals would enable more
374 accurate investigation of the reactivated contents in the future.

375

376 **TDA Reactivations during SWRs Operate Independently of Spatial Replays**

377 Numerous studies have consistently shown that hippocampal place cells are sequentially
378 reactivated within a brief time window during a SWR event, reflecting previously
379 experienced trajectories (*6-8*). Additionally, recent research indicates that the quantity of
380 reward or value associated with different locations modulates spatial reactivations both
381 quantitatively and qualitatively in the hippocampus (*10-14*). For instance, replayed
382 trajectories tend to favor locations associated with greater rewards (*11*) or higher value
383 rewards (*14*). Similarly, the frequency of SWRs and spatial replays adjusts to reflect the
384 relative magnitude of reward between two ends of a linear track (*10*). Furthermore, studies
385 have demonstrated that firing rate differences related to the animal's running directions or
386 environmental contexts are preserved in spatial replay patterns within hippocampal SWRs
387 (*18,19*).

388 While the aforementioned studies focus on how task-relevant variables influence
389 spatial reactivations during SWRs, our present study highlights the neural reactivation of
390 TDA information during SWRs, occurring independently of spatial reactivations. The
391 likelihood of a neuron representing both spatial and task-relevant factors simultaneously is
392 very low in both the hippocampus and subiculum. Specifically, we found that only 3.4% of
393 CA1 SWRs exhibited both spatial and TDA reactivations, whereas approximately 40%
394 involved TDA reactivations and 20% involved spatial reactivations in CA1 (**Figures 5B** and
395 **7B**). This phenomenon was more pronounced in the subiculum, where just 1.2% of SWRs
396 showed concurrent spatial and TDA reactivations compared to CA1. Moreover, in the
397 subiculum, the proportion of MF cells per SWR increased during TDA reactivations (**Figure**
398 **7B**) and decreased during spatial reactivations (**Figure 8D**).

399 Our findings suggest that TDA variables, such as surrounding visual scenes and
400 upcoming choice arms, are reinstated during SWRs in both the hippocampus and subiculum
401 by recruiting neural ensembles with similar selective firing patterns, independent of their
402 spatial representations on the track. This discovery opens new avenues for investigating
403 SWR-related reactivation patterns of neurons recorded from various regions of the
404 hippocampal formation (e.g., subiculum, intermediate hippocampus) whose spatial correlates
405 are not as precisely tuned as the typical place cells found in the dorsal hippocampus.

406

407 **The Functional Significance of TDA Reactivation in the Subiculum**

Previous research has shown that hippocampal SWRs are transmitted to the granular retrosplenial cortex via the subiculum (*26*). However, we found that fewer TDA reactivations occur in the CA1 than in the subiculum (**Figure 5B**), though a significant proportion still happens in the CA1. Building on this evidence, we suggest that the subiculum not only helps propagate hippocampal SWRs to cortical regions but also amplifies and transmits signals carrying TDA variables to cortical areas during hippocampal-dependent memory tasks. Another possibility is that TDA reactivations could originate within the subiculum itself and then propagate to the hippocampal formation, as independently generated SWRs have been reported in the subiculum (*27*). However, since the back-projection from the subiculum to CA1 is known to function under limited task demands, such as object-in-place memory (*41,42*), this hypothesis needs further testing.

It is important to note that TDA reactivations were observed in the awake state, specifically during behavioral tasks when rats were actively engaged. Unlike ripples during slow-wave sleep, which are thought to play a role in the consolidation of hippocampal episodic memory (*20,21,43,44*), awake ripples are considered important for active route planning or path simulation to reach goal locations in an environment (*45-47*). Disruptions of awake ripples have been shown to impair memory-guided navigational tasks (*21*). The TDA reactivations observed in our current study may also facilitate the prediction or simulation of visual scene stimuli as cues for upcoming choice arms or required responses to reach goal locations.

On the other hand, consistent with prior studies, spatial replay was predominant in the CA1 (**Figure 8**). Moreover, these spatial reactivations likely propagate while bypassing the subiculum. The poorer spatial tuning of subicular place cells compared to those in the CA1 (*30-34*) may intuitively explain the relative rarity and less robustness of spatial replay in the subiculum. Some recent papers have argued that the subiculum and CA1 possess similar levels of spatial information (when measured in information per second) (*29, 33*). Additionally, there was no significant difference in the decoding performance of the animal's position between the two regions (*29*). Nevertheless, the analysis was based on neural activities recorded while running on the track, so it remains unclear whether the subiculum and CA1 have the same level of spatial representation during the short time window of SWR.

Overall, TDA reactivations are primarily driven by MF cells in the subiculum, which are expected to receive convergent input from single place cells in the CA1 and then transmit this information to cortical and subcortical regions associated with goal-directed behavior or motivation. This is supported by previous reports that TDA representations, such as the prospective coding of choice arm on a T-maze, were particularly observed at high rates in NAC-projecting neurons in the subiculum, and that these NAC-projecting neurons enhanced their activities during SWRs (*29*). Therefore, we propose that the subiculum and CA1 cooperate to organize neural network activities during SWRs by transmitting spatial or TDA variables in a complementary manner. Furthermore, the subiculum reactivates multiple types of TDA information within a single SWR event, potentially enhancing associative learning by integrating and multiplexing heterogeneous task-related factors, as suggested by our earlier study (*34*).

## Materials and Methods

### Subjects

The current study used five Long-Evans male rats, each weighing 350-400 g. Food was restricted to keep their body weight at 85% of their free-feeding weight and to maintain their motivation during the behavioral task while water was available ad libitum. The rats were individually housed and kept on a 12-hour light/dark cycle. All procedures were carried out under the guidelines set by the Institutional Animal Care and Use Committee (IACUC) of Seoul National University (SNU-200504-3-1).

### Behavioral task

Our previous studies (*32,34*) provide a detailed description of experimental procedures, including the visual scene memory (VSM) task and the apparatus. Briefly, rats were required to make a left or right turn on the T-maze according to the patterned visual stimulus (i.e., visual scene) presented on the LCD monitors surrounding the arms. Before the initiation of each trial, the rat was placed in a start box enclosed by black walls (22.5 x 16 cm, 31.5 cm height). Upon the experimenter's opening of the start box's guillotine door, the rat was

exposed to one of four visual scene stimuli displayed on an array of three adjacent LCD monitors, signaling the onset of the trial. Then, the rat ran along the stem of the T-maze (73 x 8 cm for stem) and had to choose left or right arm (38 x 8 cm for arms) at the end of the stem (i.e., "choice point") based on the visual scene. If the rat chose the correct arm, it received a quarter piece of cereal reward (Froot Loops, Kellogg's) from the food well at the end of the arm. If it chose the wrong arm, no reward was given. After making a correct or wrong choice, the rat returned to the start box, and the door was closed to prevent the rat from seeing outside during the inter-trial interval (ITI) period before the start of the subsequent trial. Four grayscale visual patterns (zebra stripes, bamboo, pebbles, mountain) were used for visual scenes. Among these four scenes, zebra stripes and bamboo patterns were associated with the left arm, while pebbles and mountain patterns were associated with the right arm in all sessions. These four visual scenes were presented in a pseudorandom sequence within a session. Data obtained from incorrect trials and subsequent ITIs was excluded from the analysis in the current study.

Before surgery, the rat learned two scene pairs sequentially (either zebra versus pebbles or bamboo versus mountain, counterbalanced across rats) until it met the performance criterion for each pair (at least 75% correct for each scene for two consecutive days, with 40 trials per session). It took the rats an average of 2 weeks (13.4 ± 0.9 sessions, mean ± STE) to meet the performance criterion for both pairs.

**Hyperdrive implantation surgery and electrophysiological recording**

Once the rat met the performance criterion, a hyperdrive equipped with 24 tetrodes and three additional reference electrodes was surgically implanted into the right hemisphere to cover an area from 3.2 to 6.6 mm posterior to bregma and 1 to 4 mm lateral to the midline. Following a week of recovery, the rat underwent retraining with two pairs of scene stimuli in order until it regained its presurgical performance levels, completing up to 160 trials. During this postsurgical retraining phase, the tetrodes were progressively lowered into the subiculum and CA1 at a rate of 40 to 160 μm per day. Once the optimal number of single units in the target regions was achieved, the main recording sessions commenced (123 ± 6 trials per session, mean ± STE).

497 Neural signals were transmitted through the headstage and tether attached to the
498 electrode interface board of the hyperdrive to the data acquisition system (Digital Lynx SX;
499 Neuralynx). Using the Digital Lynx system, neural signals measured by tetrodes are amplified
500 1,000-10,000 times and digitized at 32 kHz. Then the signals were filtered at 600-6,000 Hz
501 for spiking data and 0.1-1,000 Hz for local field potential (LFP) data.

502

503 **Histological verification of electrode tip positions**

504 After all recordings were completed, an electrolytic lesion was performed on each tetrode
505 (10μA for 10 s) to mark the tip position. After 24 hours, the rat was euthanized by inhaling a
506 lethal dose of carbon dioxide ($CO_2$) and perfused transcardially. After post-fixation
507 procedures, the coronal brain sections, which were 40 μm in thickness, were stained with
508 thionin and by Timm's method. Electrode tip positions were verified using a series of brain
509 sections, considering the presurgical electrode configuration and electrolytic lesion marks
510 (see details in our previous paper (*32*)). The anatomical boundaries of the CA1 and
511 subiculum were established by referencing a rat brain atlas (*48*). Electrodes placed in the
512 CA1-subiculum transition zone were excluded from further examination.

513

514 **Unit isolation and filtering**

515 Single units were manually isolated using both commercial software (SpikeSort3D;
516 Neuralynx) and a custom-written program (WinClust), based on waveform parameters such
517 as peak amplitude and energy. Units qualified for analysis if they exhibited an average peak-
518 to-valley amplitude greater than 75μV and had less than 1% of spikes occurring within the
519 refractory period (< 1 ms). Fast-spiking units, characterized by an average firing rate over
520 10Hz and an average waveform width of less than 325μs, were excluded from the analysis.
521 Adhering to these criteria, complex-spiking units (n=192 in the subiculum, n=282 in CA1)
522 were finally included in the current study.

523

524 **Construction of linearized firing rate maps**

525 For the position data collected during the outbound period of each trial (from leaving the start

box to reach the food well), we binned the position data into 2cm-sized spatial bins. For each spatial bin between stem and arm, we tested significance of trace divergence (difference in animal position along the arm axis, two-sample *t*-test) between trials to the left arm and trials to the right arm. A choice point was defined when at least two consecutive spatial bins showed a significant trace difference. For the intersection (from the choice point to arms), the animal position was linearized to one-dimensional coordinates, considering both the animal's x and y positions, and the spatial bins were fitted with a triangular shape along the animal's trace. Then, we created a linearized firing rate map by dividing the number of spikes by the number of position data (recorded 30 times per second) for each bin. The linearized firing rate map was smoothed for display using an adaptive binning method (*49*).

**Identification of spiking theta phases**

The recorded LFP data was down-sampled to 2kHz and then filtered using a 3-300Hz bandpass filter (third-order butterworth filter via *filtfilt* function in Matlab). For each tetrode, we applied the power spectral density (PSD) function using the multi-taper method (Chronux ToolBox; Matlab) and selected the reference electrode with the strongest power in the high theta band (7-12 Hz) for each session and region (subiculum and CA1, respectively). High theta band range was chosen to minimize artifacts like bumping noise. Then, the LFP data of the reference electrode was filtered in the theta band (7-12 Hz). To obtain spiking theta phases, LFP data during outbound running epoch on the track were parsed (speed > 20cm/s). The theta phase of the reference tetrode at the moment a spike occurred was adopted as the theta phase of the spike.

**Theta-phase-based field identification**

Place fields in the subiculum and CA1 were identified by the analytical method used in our previous study (*34*), which is based on the spiking phase relationship called theta phase precession (*50,51*). To identify a group of spikes consisting of a single cycle of theta phase precession from the entire spiking activities on the outbound journey on the T-maze, we used a density-based, non-parametric clustering algorithm called DBSCAN (*52*). First, the theta phases of spikes were plotted by position on the outbound track for each complex-spiking

cell. Then, the algorithm detected a cluster of spikes based on the predetermined parameters, such as the distance (ε) between spike points and the minimum number of points ($N_{min}$) within that distance. In clustering, a core point was identified if there are more than $N_{min}$ data points within a radius of ε. Points within this radius were termed border points. Points outside this radius without neighboring core points were classified as noise points. A cluster consisted of a core point and its border points, and intersecting clusters were regarded as a single entity. Clusters with insufficient spike count less than 30, or irregular cluster shape were excluded, and the remaining clusters were used for rate modulation analysis as 'θ-phase-based place fields. ' Only cells with at least one θ-phase-based field were used for SWR detection and reactivated ensemble analysis (168 cells in the CA1, 135 cells in the subiculum). The width of each firing field was calculated by multiplying the number of bins within the place field by the spatial bin size (2 cm).

**Rate modulation analysis**

To quantify the firing rate differences between trial conditions (i.e., visual scenes or upcoming choice arms) within a place field, we calculated the selectivity index (SI):

$$\text{Selectivity index} = \frac{mean(FR_1) - mean(FR_2)}{SD(FR_1, FR_2)}$$

where $FR_1$ and $FR_2$ denote the in-field firing rates of the trials associated with two different conditions. For the selectivity index between choice directions (choice selectivity index; CSI), $FR_1$ was used for the in-field firing rate in the left choice trials, while $FR_2$ was used for the right choice trials. CSI was computed based on spiking activities up to the choice point on the track, in order to isolate the influence of upcoming directions and minimize the impact of confounding variables like varying positions. In addition, we excluded subfields from CSI calculation if their peak firing locations were fell within track arms. For the selectivity indices between visual scene stimuli, we computed two distinct scene selectivity indices (SSI): one for the pair of scenes associated with left arm choice ($SSI_L$; for the zebra-bamboo scene pair) and another for the pair associated with right arm choice ($SSI_R$; for the pebbles-mountain scene pair). These calculations included data from both the choice point and track arms. A field was excluded from further analysis for a certain condition if its selectivity index

for that condition fell between -0.1 and 0.1. The representative selectivity index of a cell for each task condition was determined as the largest (negative or positive) value of the selectivity indices of all survived fields of the cell.

**Firing rate-based field identification**

The boundaries of a rate-based place field were identified as the first spatial bin at which the firing rate 33% or less of the peak firing rate for two consecutive bins. If a local peak exceeding 50% of the maximum peak firing rate was found outside the previously defined firing field, it was considered to be the peak of another potential field. The boundaries of that field were then determined using the same method.

The spatial information score was computed according to following equation (*49*)

$$\text{Spatial information score} = \sum_i p_i \frac{\lambda_i}{\lambda} \log_2 \frac{\lambda_i}{\lambda} \text{ (bits/spike)}$$

where $i$ denotes each spatial bin, $p_i$ means the occupancy rate in the $i^{th}$ spatial bin, $\lambda_i$ means the mean firing rate in the $i^{th}$ spatial bin, and $\lambda$ means the overall mean firing rate on the track. The peak and mean firing rates of cells were calculated from the raw firing rate maps. Firing fields that met the following criteria were finally defined as 'rate-based place fields': (1) the peak firing rate was greater than 1 Hz, and (2) the spatial information score was greater than 0.5.

**Sharp-wave ripple detection**

SWRs were detected using LFP signals recorded from representative tetrodes targeting the subiculum (for subicular SWRs) and the CA1 (for CA1 SWRs), which were filtered with a 150-250 Hz band-pass filter. Initially, the tetrode exhibiting the highest ripple band power during the ITI was selected as the representative tetrode for each session and region. The Hilbert transform was then applied to obtain the envelope of the ripple band activity from this representative tetrode. Subsequently, SWR events were identified as segments exceeding 2 standard deviations (SDs) from the mean of the filtered signals. The boundaries of each SWR event were extended to include sections above mean + 0.5 SD (mean and SD were computed

613 for each session's envelope during ITI). When two SWR events occurred within intervals
614 shorter than 20 ms, they were merged into a single event. SWRs with durations shorter than
615 40 ms or longer than 200 ms were excluded from the analysis. SWR events were further
616 refined based on the number of cells reactivated during the event for TDA or spatial
617 reactivation analysis. CA1 SWRs were characterized as events where at least three CA1 cells
618 were reactivated within the SWR duration. Similarly, subicular SWRs were identified as
619 events where a minimum of three subicular cells were reactivated. The participation rate of
620 each cell in SWRs was quantified as the ratio of SWRs that elicited at least one spike from
621 the cell to the total number of SWRs recorded in the session.

622

623 **Identification for TDA reactivation**

624 To determine the reactivation of TDA information by the cell ensemble during SWRs, we
625 assessed whether the cells' representative selectivity indices exhibited a significant bias
626 toward a specific trial condition. To test this, the proportion of cells with a positive selectivity
627 index and the proportion of cells with a negative selectivity index were calculated in the
628 simultaneously recorded cell ensemble. Then, a binomial test was conducted to determine
629 whether the proportion of positive-negative selective cells in the reactivated ensemble could
630 occur at the chance level when comparing to the ensemble-level proportion. Reactivated
631 ensembles with $p < 0.05$ in the binomial test were defined as TDA reactivations.

632

633 **Identification for spatial reactivation**

634 To examine spatial reactivation, the Bayesian decoding algorithm (*53,54*) was applied to
635 reconstruct the rat's position on the track from the spiking activities in SWRs. In Bayesian
636 decoding analysis, the duration of each SWR event was divided into 10-ms temporal bins.
637 For individual bins with at least one spike, the conditional probability P(x|n) that the animal
638 is located at x when the spike count is n was given by following formula:

639 $$P(x|n) = \frac{P(n|x)P(x)}{P(n)}$$

640 where P(n) is the probability that the spike count is n, and P(x) is the probability that the

animal is positioned at x. Assuming that each cell i exhibited firing characteristics that follow a Poisson distribution and that all N cells were active independently, P(n|x) was calculated as follows:

$$\mathrm{P(n|x)} = \prod_{i=1}^{N} P(n_i|x)$$

Consequently, P(x|n) was computed as follows:

$$P(x|n) = \frac{\prod_{i=1}^{N} P(n_i|x)\, P(x)}{P(n)}$$

The strength of spatial reactivation was quantified as an $R^2$ value, obtained through linear regression performed on the decoded spatial probability distribution across temporal bins. To assess statistical significance, $R^2$ values were also obtained from shuffled data, created by randomizing the cell IDs of spikes fired during SWRs. The shuffling procedure was repeated 2,000 times, and the p-value was determined by the proportion of shuffled $R^2$ values greater than the actual value. SWRs with p-values less than 0.05 were considered to exhibit spatial reactivation.

**Statistical analysis**

Both behavioral and neural data were analyzed using a statistical significance of $\alpha = 0.05$. The one-sample Wilcoxon signed rank test was used only for the significance test of behavioral performance (75% correct choices); all other statistical tests were performed using the two-sided Wilcoxon rank-sum test. Proportional differences between cell types (i.e., SF vs. MF) and SWR types were tested using the chi-squared test. To examine the effect of region and cell type on cell firing activities, selectivity indices, or SWR participation rates, 2-way ANOVA was conducted, and unpaired two-sample t-test with Bonferroni correction was used as a post hoc test.

## References


1. H. Eichenbaum, N. J. Cohen, From conditioning to conscious recollection: Memory systems of the brain. (Oxford university press, 2004).

2. L. R. Squire, C. E. Stark, R. E. Clark, The medial temporal lobe. *Annu. Rev. Neurosci*. **27**, 279-306 (2004).

3. L. R. Squire, L. Genzel, J. T. Wixted, R. G. Morris, Memory consolidation. *Cold Spring Harb Perspect Biol* **7**, a021766 (2015).

4. G. Buzsáki, Two-stage model of memory trace formation: a role for "noisy" brain states. *Neuroscience* **31**, 551-570 (1989).

5. G. Buzsaki, Hippocampal sharp wave-ripple: A cognitive biomarker for episodic memory and planning. *Hippocampus* **25**, 1073-1188 (2015).

6. D. J. Foster, M. A. Wilson, Reverse replay of behavioural sequences in hippocampal place cells during the awake state. *Nature* **440**, 680-683 (2006).

7. K. Diba, G. Buzsaki, Forward and reverse hippocampal place-cell sequences during ripples. *Nat Neurosci* **10**, 1241-1242 (2007).

8. M. P. Karlsson, L. M. Frank, Awake replay of remote experiences in the hippocampus. *Nat Neursci* **12**, 913-918 (2009).

9. M. P. Karlsson, L. M. Frank, Network dynamics underlying the formation of sparse, informative representations in the hippocampus. *J Neurosci* **28**, 14271-14281 (2008).

10. R. E. Ambrose, B. E. Pfeiffer, D. J. Foster, Reverse Replay of Hippocampal Place Cells Is Uniquely Modulated by Changing Reward. *Neuron* **91**, 1124-1136 (2016).

11. F. Michon, J.-J. Sun, C. Y. Kim, D. Ciliberti, F. Kloosterman, Post-learning hippocampal replay selectively reinforces spatial memory for highly rewarded locations. *Curr Biol* **29**, 1436-1444 (2019).

12. C. T. Wu, D. Haggerty, C. Kemere, D. Ji, Hippocampal awake replay in fear memory retrieval. *Nat Neurosci* **20**, 571-580 (2017).

13. J. Ormond, S. A. Serka, J. P. Johansen, Enhanced reactivation of remapping place cells during aversive learning. *J Neurosci* **43**, (2023).

14. S. W. Jin, H. S. Ha, I. Lee (in press), Selective reactivation of value- and place-dependent information during sharp-wave ripples in the intermediate and dorsal hippocampus. *Sci Adv* (2024).

15. A. S. Gupta, M. A. van der Meer, D. S. Touretzky, A. D. Redish, Hippocampal replay is not a simple function of experience. *Neuron* **65**, 695-705 (2010).

16. J. Widloski, D. J. Foster, Flexible rerouting of hippocampal replay sequences around changing barriers in the absence of global place field remapping. *Neuron* **110**, 1547-1558 (2022).

17. X. Wu, D. J. Foster, Hippocampal replay captures the unique topological structure of a novel environment. *J Neurosci* **34**, 6459-6469 (2014).

18. C. D. Schwindel, Z. Navratilova, K. Ali, M. Tatsuno, B. L. McNaughton, Reactivation of Rate Remapping in CA3. *J Neurosci* **36**, 9342-9350 (2016).

19. M. Tirole, M. H. Gorriz, M. Takigawa, L. Kukovska, D. Bendor, Experience-Driven Rate Modulation is Reinstated During Hippocampal Replay. *Elife* **11**, e79031 (2022).

20. G. Girardeau, K. Benchenane, S. I. Wiener, G. Buzsaki, M. B. Zugaro, Selective suppression of hippocampal ripples impairs spatial memory. *Nat Neurosci* **12**, 1222-1223 (2009).

21. S. P. Jadhav, C. Kemere, P. W. German, L. M. Frank, Awake hippocampal sharp-wave ripples support spatial memory. *Science* **336**, 1454-1458 (2012).

22. J. H. Sadowski, M. W. Jones, J. R. Mellor, Sharp-Wave Ripples Orchestrate the Induction of Synaptic Plasticity during Reactivation of Place Cell Firing Patterns in the Hippocampus. *Cell Rep* **14**, 1916-1929 (2016).

23. A. Fernández-Ruiz et al., Long-duration hippocampal sharp wave ripples improve memory. *Science* **364**, 1082-1086 (2019).

24. I. Gridchyn, P. Schoenenberger, J. O'Neill, J. Csicsvari, Assembly-Specific Disruption of Hippocampal Replay Leads to Selective Memory Deficit. *Neuron* **106**, 291-300 (2020).

25. A. D. Grosmark, F. T. Sparks, M. J. Davis, A. Losonczy, Reactivation predicts the consolidation of unbiased long-term cognitive maps. *Nat Neurosci* **24**, 1574-1585 (2021).

26. N. Nitzan et al., Propagation of hippocampal ripples to the neocortex by way of a subiculum-retrosplenial pathway. *Nat Commun* **11**, 1947 (2020).

27. B. Imbrosci et al., Subiculum as a generator of sharp wave-ripples in the rodent hippocampus. *Cell Rep* **35**, 109021 (2021).

28. C. Bohm et al., Functional Diversity of Subicular Principal Cells during Hippocampal Ripples. *J Neurosci* **35**, 13608-13618 (2015).

29. T. Kitanishi, R. Umaba, K. Mizuseki, Robust information routing by dorsal subiculum neurons. *Sci Adv* **7**, eabf1913 (2021).

30. P. E. Sharp, C. Green, Spatial correlates of firing patterns of single cells in the subiculum of the freely moving rat. *J Neurosci* **14**, 2339-2356 (1994).

31. S. M. Kim, S. Ganguli, L. M. Frank, Spatial information outflow from the hippocampal circuit: distributed spatial coding and phase precession in the subiculum. *J Neurosci* **32**, 11539-11558 (2012).

32. H. W. Lee, S. M. Lee, I. Lee, Neural Firing Patterns Are More Schematic and Less Sensitive to Changes in Background Visual Scenes in the Subiculum than in the Hippocampus. *J Neurosci* **38**, 7392-7408 (2018).

33. D. Ledergerber et al., Task-dependent mixed selectivity in the subiculum. *Cell Rep* **35**, (2021).

34. S. M. Lee, J. M. Seol, I. Lee, Subicular neurons represent multiple variables of a hippocampal-dependent task by using theta rhythm. *PLoS Biol* **20**, e3001546 (2022).

35. S. Kim, J. Lee, I. Lee, The hippocampus is required for visually cued contextual response selection, but not for visual discrimination of contexts. *Front Behav Neurosci* **6**, 66 (2012).

36. S. M. Lee, J. Shin, I. Lee, Significance of visual scene-based learning in the hippocampal systems across mammalian species. *Hippocampus* **33**, 505-521 (2022).

37. P. D. Rich, H.-P. Liaw, A. K. Lee, Large environments reveal the statistical structure governing hippocampal representations. *Science* **345**, 814-817 (2014).

38. H. J. Spiers, R. M. Hayman, A. Jovalekic, E. Marozzi, K. J. Jeffery, Place field repetition and purely local remapping in a multicompartment environment. *Cereb Cortex* **25**, 10-25 (2015).

39. B. Harland, M. Contreras, M. Souder, J. M. Fellous, Dorsal CA1 hippocampal place cells form a multi-scale representation of megaspace. *Curr Biol* **31**, 2178-2190 (2021).

40. S. Tanni, W. de Cothi, C. Barry, State transitions in the statistically stable place cell population correspond to rate of perceptual change. *Curr Biol* **32**, 3505-3514 (2022).

41. Y. Sun et al., Cell-type-specific circuit connectivity of hippocampal CA1 revealed through Cre-dependent rabies tracing. *Cell Rep* **7**, 269-280 (2014).

42. Y. Sun et al., CA1-projecting subiculum neurons facilitate object–place learning. *Nat Neurosci* **22**, 1857-1870 (2019).

43. B. Shen, B. L. McNaughton, Modeling the spontaneous reactivation of experience-specific hippocampal cell assembles during sleep. *Hippocampus* **6**, 685-692 (1996).

44. G. M. van de Ven, S. Trouche, C. G. McNamara, K. Allen, D. Dupret, Hippocampal Offline Reactivation Consolidates Recently Formed Cell Assembly Patterns during Sharp Wave-Ripples. *Neuron* **92**, 968-974 (2016).

45. M. F. Carr, S. P. Jadhav, L. M. Frank, Hippocampal replay in the awake state: a potential substrate for memory consolidation and retrieval. *Nat Neurosci* **14**, 147-153 (2011).

46. A. C. Singer, M. F. Carr, M. P. Karlsson, L. M. Frank, Hippocampal SWR activity predicts correct decisions during the initial learning of an alternation task. *Neuron* **77**, 1163-1173 (2013).

47. B. E. Pfeiffer, D. J. Foster, Hippocampal place-cell sequences depict future paths to remembered goals. *Nature* **497**, 74-79 (2013).

48. G. Paxinos, C. Watson, The rat brain in stereotaxic coordinates: hard cover edition. (Elsevier, 2006).

49. W. Skaggs, B. Mcnaughton, K. Gothard, An information-theoretic approach to deciphering the hippocampal code. *Adv Neural Inf Process Syst* 5, 1030-1038 (1992).

50. J. O'Keefe, M. L. Recce, Phase relationship between hippocampal place units and the EEG theta rhythm. *Hippocampus* **3**, 317-330 (1993).

51. A. P. Maurer, S. L. Cowen, S. N. Burke, C. A. Barnes, B. L. McNaughton, Organization of hippocampal cell assemblies based on theta phase precession. *Hippocampus* **16**, 785-794 (2006).

52. M. Ester, H. Kriegel, J. Sander, X. Xu, A density-based algorithm for discovering clusters in large spatial databases with noise, in *Proceedings of the Second International Conference on Knowledge Discovery and Data Mining* (AAAI, 1996), vol. 240, p. 6.

53. E. N. Brown, L. M. Frank, D. Tang, M. C. Quirk, M. A. Wilson, A statistical paradigm for neural spike train decoding applied to position prediction from ensemble firing patterns of rat hippocampal place cells. *J Neurosci* **18**, 7411-7425 (1998).

54. K. Zhang, I. Ginzburg, B. L. McNaughton, T. J. Sejnowski, Interpreting neuronal population activity by reconstruction: unified framework with application to hippocampal place cells. *J Neurophysiol* **79**, 1017-1044 (1998).

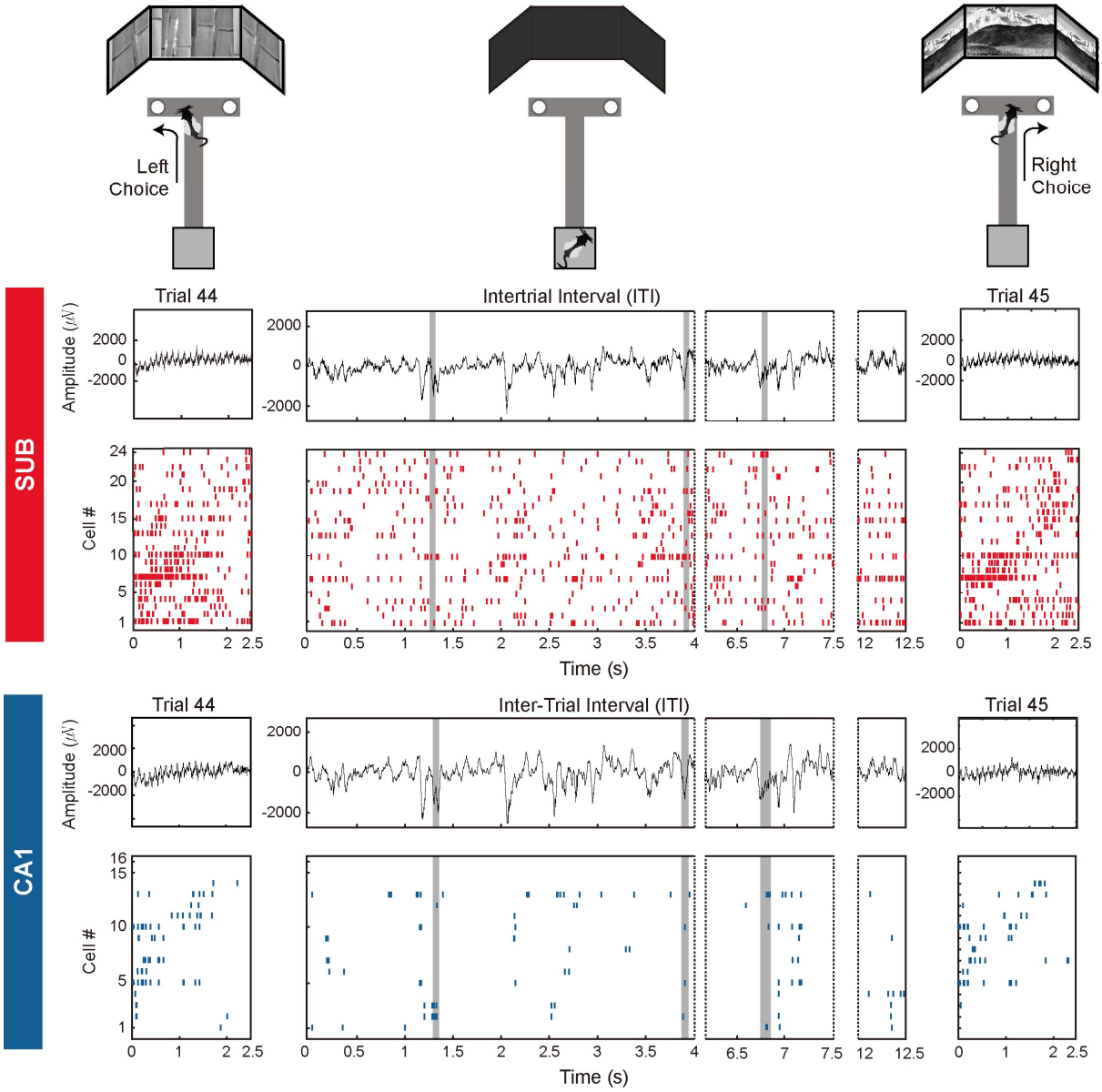


**Figure 1. SWR detection in the subiculum and CA1 during the visual scene memory task**

Top: Illustration of trial epochs and inter-trial interval in the visual scene memory task. During each trial epoch, the rat was required to choose left or right arm associated with the visual scene presented on the monitors at the end of the stem to obtain a cereal reward from the food well at the end of the arm. Once the rat returned to the start box, a guillotine door closed, requiring the rat to stay inside the start box for about 10 seconds. Bottom: Local field potential (LFP) and spiking activities of cell ensembles recorded in the subiculum and CA1 simultaneously during an example inter-trial interval (ITI) and the preceding and subsequent trials (trials 44 and 45, from rat 232-07 session). In the center column, SWR events are indicated by gray shades. In each region, cells are sorted by on-track field peak positions. SUB, subiculum.

804

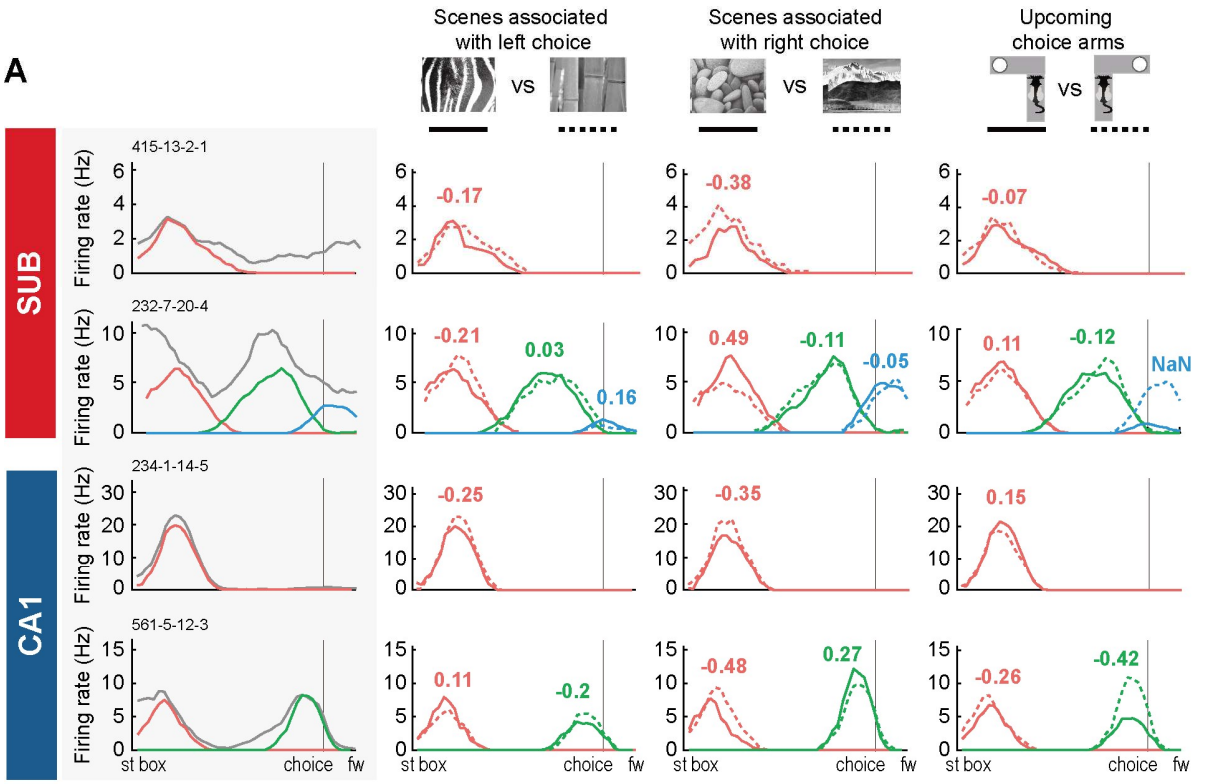
A
Scenes associated with left choice
vs
Scenes associated with right choice
vs
Upcoming choice arms
vs
SUB
CA1
415-13-2-1
232-7-20-4
234-1-14-5
561-5-12-3
Firing rate (Hz)
-0.17
-0.38
-0.07
-0.21
0.03
0.16
0.49
-0.11
-0.05
0.11
-0.12
NaN
-0.25
-0.35
0.15
0.11
-0.2
-0.48
0.27
-0.26
-0.42
st box
choice
fw

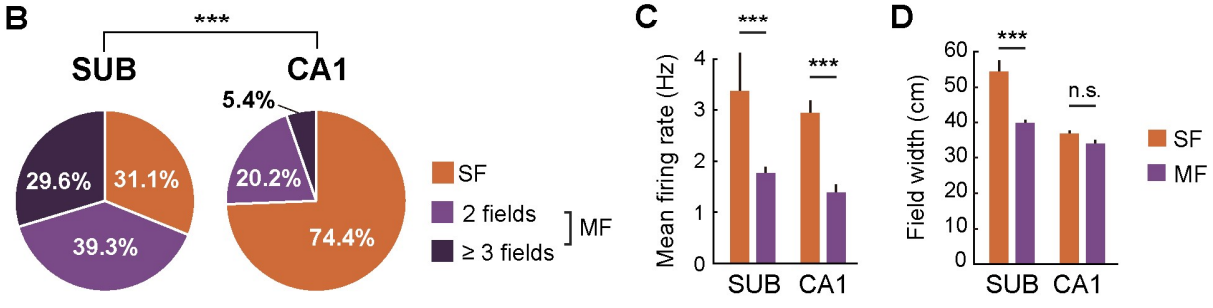
B
***
SUB
CA1
5.4%
29.6%
31.1%
39.3%
20.2%
74.4%
SF
2 fields
≥ 3 fields
MF
C
Mean firing rate (Hz)
***
***
SUB
CA1
D
Field width (cm)
***
n.s.
SUB
CA1
SF
MF

805

**Figure 2. Rate modulation of θ-phase-based fields by scene and choice**

**(A)** Each row displays an example cell from the subiculum and CA1. In the first column of each row (gray-shaded) is the linearized firing rate map on the T-maze, averaged over all trials. Overall firing activities are shown as gray lines, while place fields defined by theta phases are shown as colored lines. The subsequent columns on the right depict firing rate maps constructed by trials associated with different TDA information (visual scenes and upcoming choice arms). In each column, the solid and dotted lines represent the average firing patterns for different scenes or choice direction, color-coded by θ-phase-based subfields. The numbers above the fields indicate the selectivity indices for the scene pairs or the upcoming choice direction (see Materials and Methods for detailed description), and the number is colored when the absolute value of selectivity index is greater than 0.1. **(B)** Difference in cell proportions between the subiculum and CA1 when cells are classified by the number of θ-phase-based fields: "SF" for single field, "MF" for multiple fields. **(C)** Comparison of mean firing rates of individual θ-phase-based fields for SF and MF cell types between the subiculum and CA1. **(D)** Comparison of field width of individual θ-phase-based fields for SF and MF cell types between the regions. *** $p<0.001$. st box, start box; fw, food well; SUB, subiculum; SF, single-field; MF, multi-field.

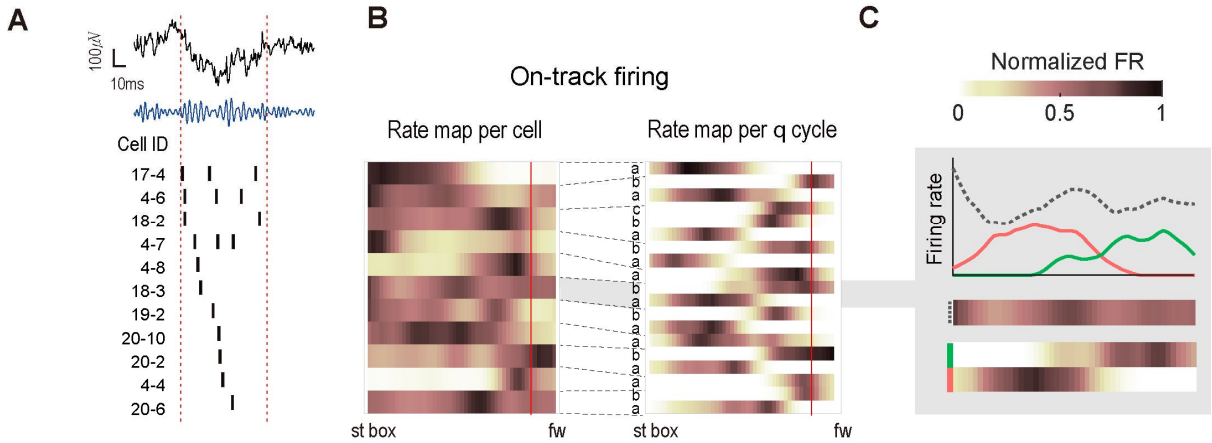


**Figure 3. θ-phase-based field parcellation of SWR-coactivated neuronal ensemble.**

**(A)** An example of subicular SWR during inter-trial interval. On the leftmost column, the raw LFP trace of a SWR event (solid black line, time and LFP amplitude indicated by the scale bar at the upper left) and 150-250Hz band-pass filtered LFP trace (solid blue line) are displayed. Dotted vertical red lines indicate the SWR boundaries. A raster plot under the traces shows spiking activities of cell ensemble coactivated during the SWR. Cells are sorted based on the order of their first spike time. The numbers on the left side of the raster plot indicate the cell ID. **(B)** Cell-based firing rate map (*rate map per cell*, left) and θ-phase-based rate map (*rate map per θ cycle*, right) constructed using all trials. Firing rates in each map are normalized by the cell's maximum firing rate. Red solid line denotes choice point. **(C)** The on-track firing activities of an example cell (18-3) in the forms of a line plot and a heatmap (normalized by peak firing rate). Gray dotted line represents overall activity, while solid, colored lines represent multiple θ-phase-based fields.

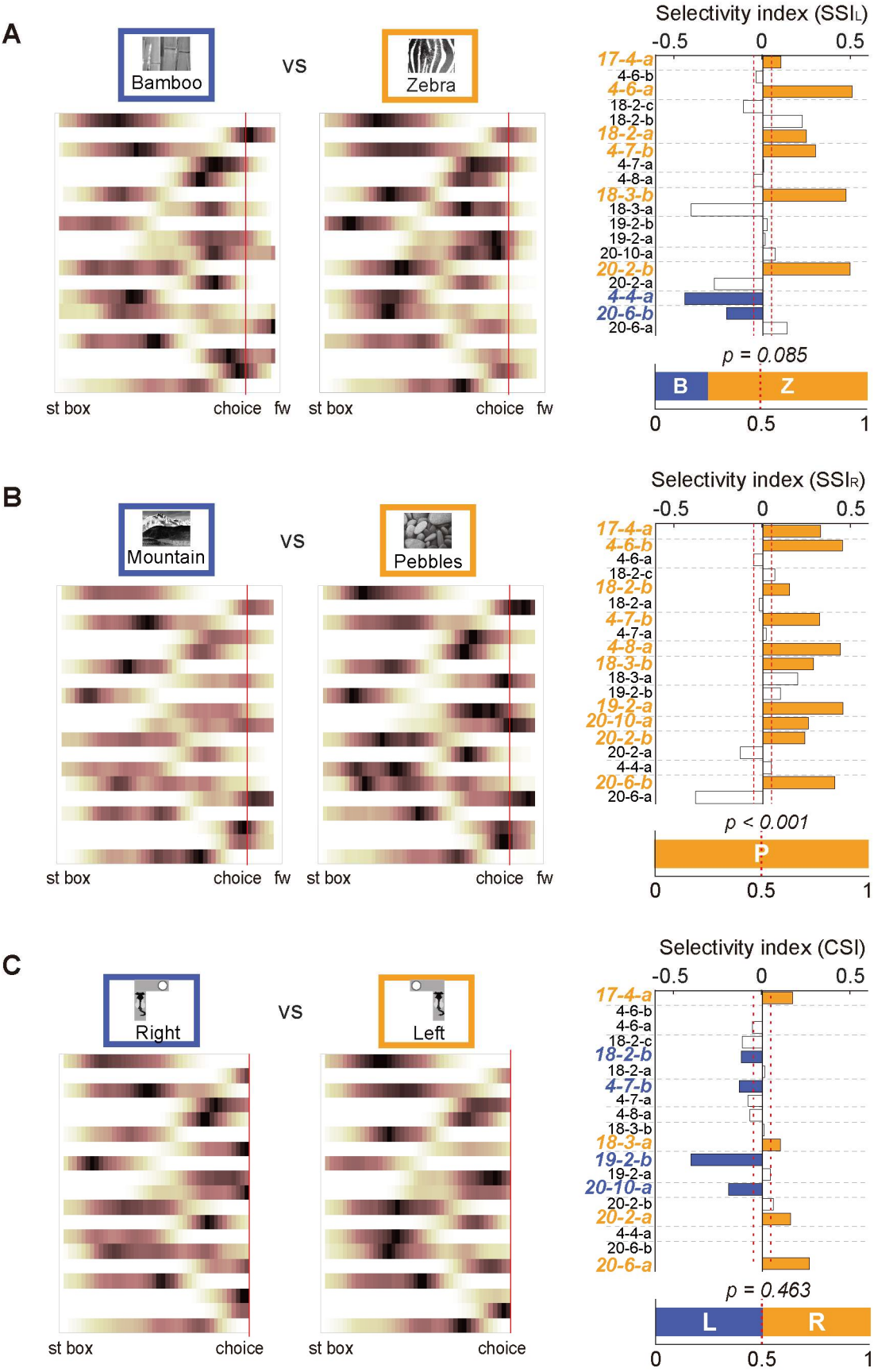
A
Bamboo
vs
Zebra
st box
choice
fw
st box
choice
fw
Selectivity index (SSIL)
-0.5
0
0.5
17-4-a
4-6-b
4-6-a
18-2-c
18-2-b
18-2-a
4-7-b
4-7-a
4-8-a
18-3-b
18-3-a
19-2-b
19-2-a
20-10-a
20-2-b
20-2-a
4-4-a
20-6-b
20-6-a
p = 0.085
B
Z
0
0.5
1
B
Mountain
vs
Pebbles
st box
choice
fw
st box
choice
fw
Selectivity index (SSIR)
-0.5
0
0.5
17-4-a
4-6-b
4-6-a
18-2-c
18-2-b
18-2-a
4-7-b
4-7-a
4-8-a
18-3-b
18-3-a
19-2-b
19-2-a
20-10-a
20-2-b
20-2-a
4-4-a
20-6-b
20-6-a
p < 0.001
P
0
0.5
1
C
Right
vs
Left
st box
choice
st box
choice
Selectivity index (CSI)
-0.5
0
0.5
17-4-a
4-6-b
4-6-a
18-2-c
18-2-b
18-2-a
4-7-b
4-7-a
4-8-a
18-3-b
18-3-a
19-2-b
19-2-a
20-10-a
20-2-b
20-2-a
4-4-a
20-6-b
20-6-a
p = 0.463
L
R
0
0.5
1

838

**Figure 4. TDA bias in the neuronal ensemble reactivation during SWR**

**(A)** (*left*) θ-phase-based rate maps that are reconstructed by left-arm-choice trials associated with the bamboo scene versus the zebra scene. The rate map of each subfield is normalized by the maximum rate for that particular scene or choice condition. (*right*) Distribution of $SSI_L$ for individual subfields. Each bar corresponds to a subfield in the rate map shown on the left panel. Dashed gray lines divide subfields from different cells. Empty bars represent selectivity indices that do not meet the criterion (dashed red lines; between -0.1 and 0.1), or that are not the highest within the cell. The bar graph at the bottom shows the proportion of cells in the reactivated ensemble selective to certain scenes or choice conditions. St box, start box; choice, choice point; fw, food well of the track; Z, zebra scene; B, bamboo scene; P, pebbles scene; M, mountain scene; L, left choice arm; R, right choice arm. **(B)** (*left*) θ-phase-based rate maps that are reconstructed by right-arm-choice trials associated with the mountain scene versus the pebbles scene. (*right*) Distribution of $SSI_R$ for individual subfields. **(C)** (*left*) θ-phase-based rate maps that are reconstructed by the trials associated with the left versus right choices. (*right*) Distribution of CSI for individual subfields.

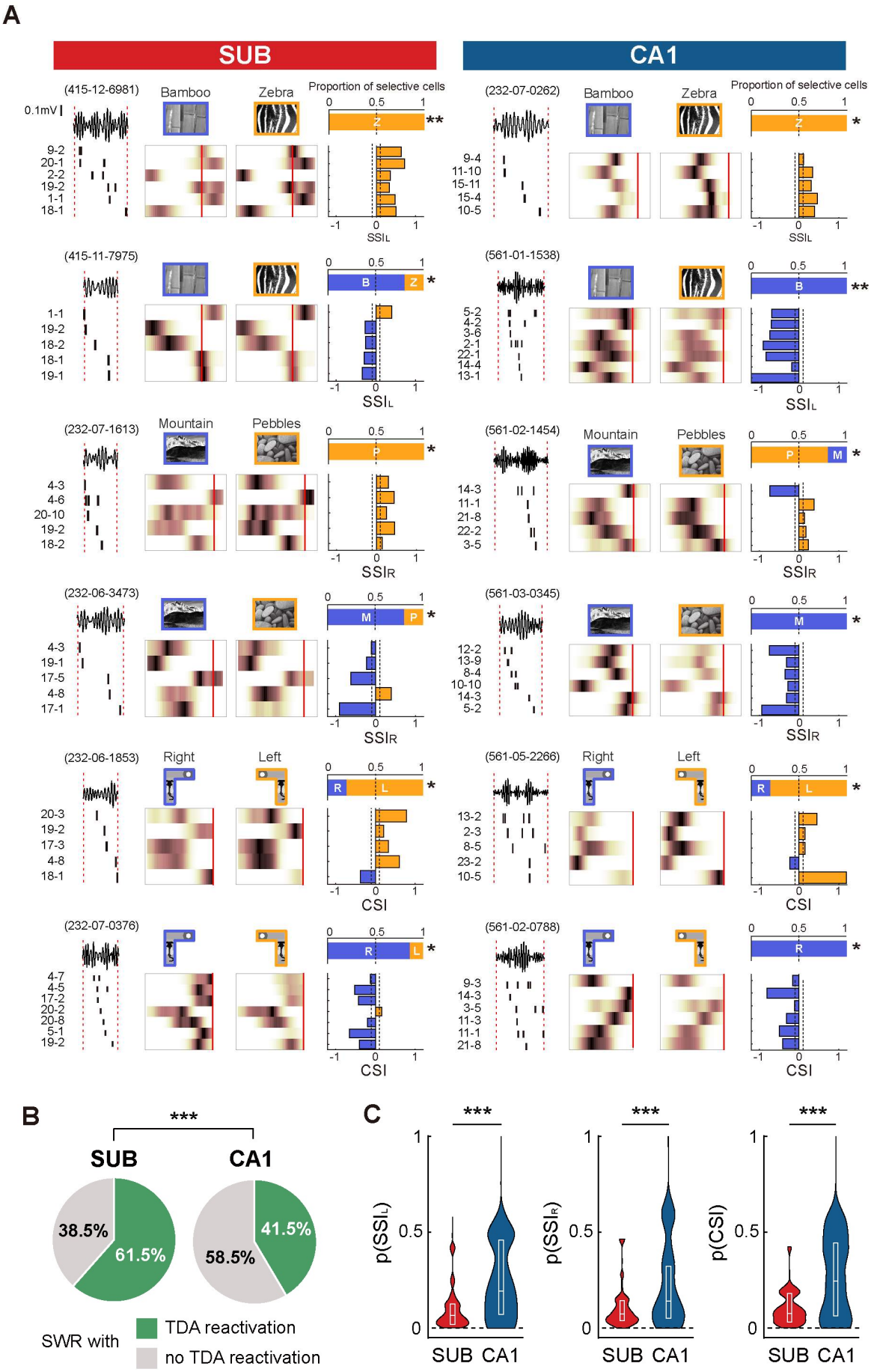
A
SUB
CA1
Proportion of selective cells
Bamboo
Zebra
Mountain
Pebbles
Right
Left
SSIL
SSIR
CSI
B
SUB
CA1
38.5%
61.5%
41.5%
58.5%
SWR with
TDA reactivation
no TDA reactivation
C
p(SSIL)
p(SSIR)
p(CSI)
SUB CA1

854

**Figure 5. TDA reactivation in SWR was more prevalent in the subiculum than in the CA1**

**(A)** Example SWRs with TDA reactivations of the subiculum (left) and the CA1 (right). In each example, the leftmost part shows filtered LFP trace and spiking activities of cell ensemble within SWR boundaries. The middle colormaps represent the on-track firing rate map of θ-phase-based subfields from which representative selectivity indices were selected for each task condition. For the example SWRs with choice reactivation, "arm" sections of T-maze, from choice point to food well, are excluded from display, since those sections are not used to calculate choice selectivity index. The top right graph depicts the proportion of cells in the reactivated ensemble that are selective to certain trial conditions. The statistical significance of ensemble-level selectivity bias calculated by a binomial test is indicated as asterisks. The bottom right bar graphs are representative selectivity indices for individual cells, color-coded by trial conditions. **(B)** Proportion of SWRs with significant TDA reactivation in each region. **(C)** Distributions of p-values obtained by the binomial test. In the inset box plot, the center line indicates median value, with the top and bottom lines denoting the 1$^{st}$ and 3$^{rd}$ quartiles, respectively. *$p$<0.05, **$p$<0.01, ***$p$<0.001. St box, start box; choice, choice point; fw, food well; Z, zebra scene; B, bamboo scene; P, pebbles scene; M, mountain scene; L, left choice arm; R, right choice arm; SUB, subiculum.

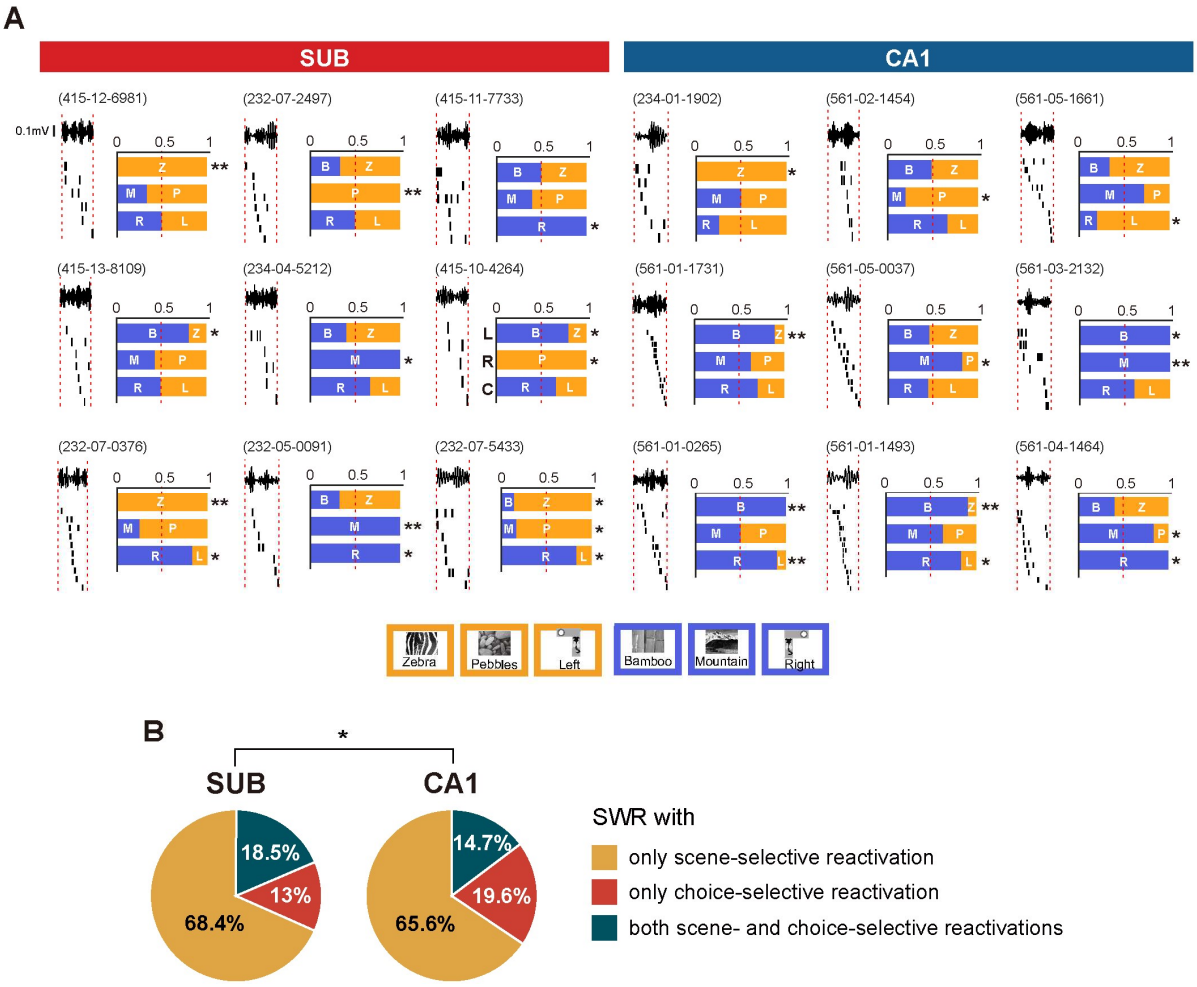





**Figure 6. SWRs representing different types of TDA information together are more prevalent in the subiculum than CA1**

**(A)** Example SWRs with scene-, choice- or both scene- and choice-selective reactivation in the subiculum (left panel) and the CA1 (right panel). In each example, the leftmost part display filtered LFP trace and spiking activities within the SWR boundaries. The horizontal bar plots on the right are the proportions of cells in the reactivated ensemble that are selective to each scene or choice information. Asterisk marks indicate the significance of proportional difference obtained from binomial tests. **(B)** Proportion of SWRs that exhibited scene-, choice- or both scene- and choice-selective reactivation within each region. *$p$<0.05, **$p$<0.01, ***$p$<0.001; Z, zebra scene; B, bamboo scene; P, pebbles scene; M, mountain scene; L, left choice arm; R, right choice arm; SUB, subiculum.

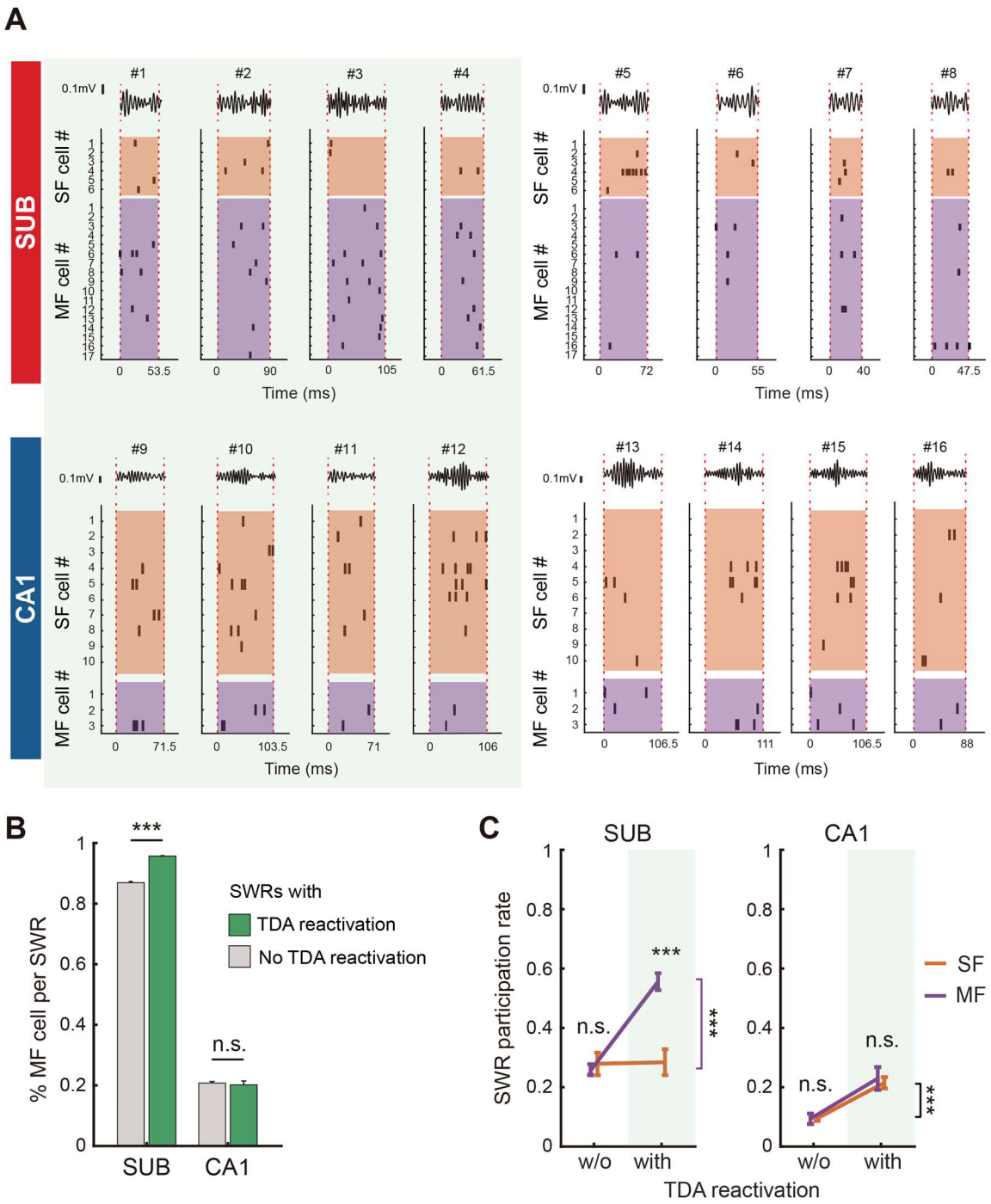


**Figure 7. Contribution of subicular MF cells to the TDA reactivation.**

**(A)** Example SWRs in the subiculum and CA1, with significant TDA reactivation (in the left shaded area) and without such reactivation (in the right). Filtered LFP traces are displayed, and spiking activities of reactivated cell ensemble are sorted by the cell type (i.e., SF and MF cells). **(B)** Proportion of MF cells per SWR event (data are presented as means ± standard error of the mean). **(C)** Comparison of SWR participation rates for individual cells between the cell types and SWR types (i.e., SWRs with or without TDA reactivation) within each region. ***$p$<0.001; SUB, subiculum. w/o, SWRs without TDA reactivation.

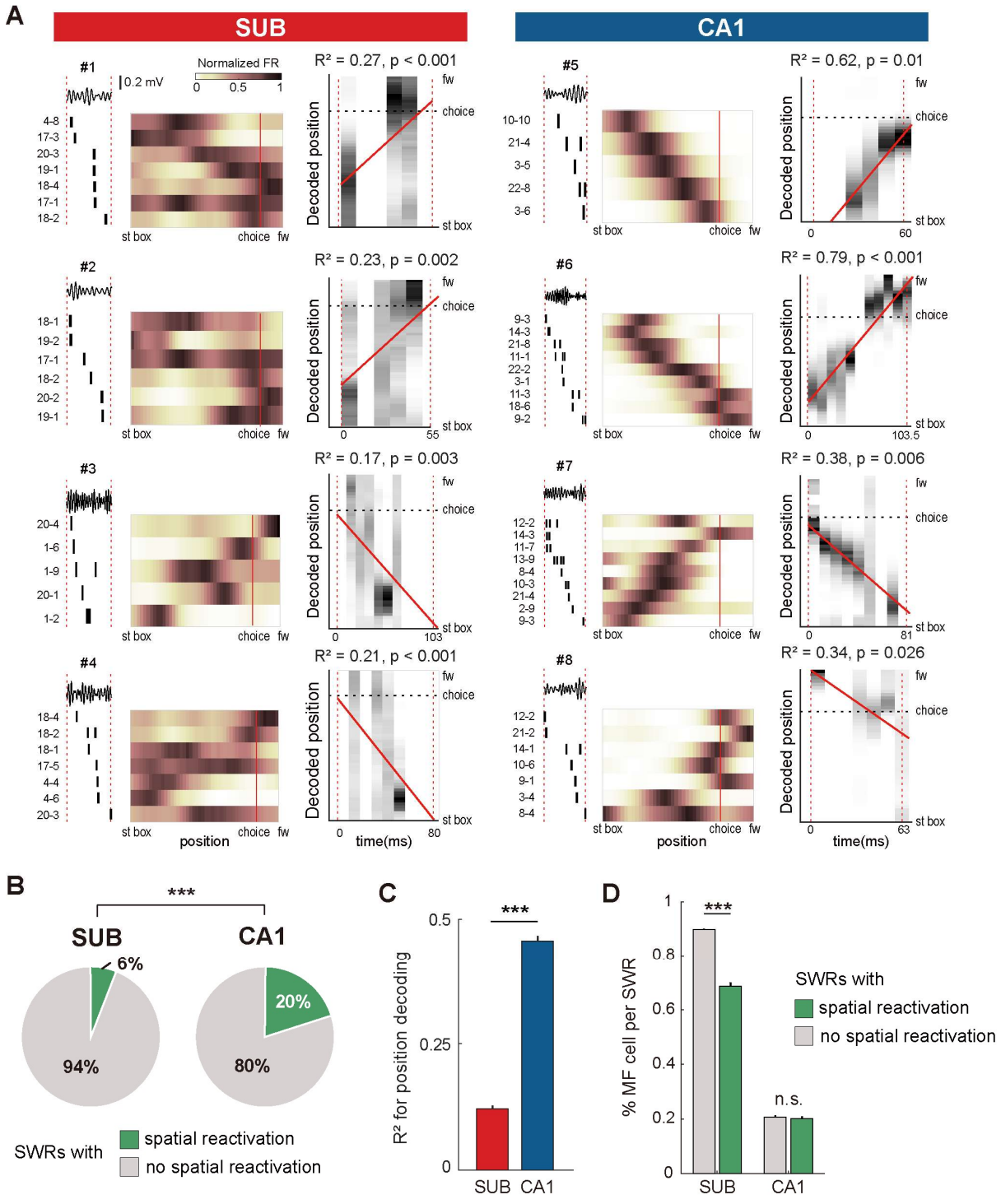
A
SUB
CA1
#1
Normalized FR
0.2 mV
0 0.5 1
R² = 0.27, p < 0.001
#2
R² = 0.23, p = 0.002
#3
R² = 0.17, p = 0.003
#4
R² = 0.21, p < 0.001
#5
R² = 0.62, p = 0.01
#6
R² = 0.79, p < 0.001
#7
R² = 0.38, p = 0.006
#8
R² = 0.34, p = 0.026
st box
choice
fw
position
time(ms)
Decoded position
B
***
SUB
CA1
6%
94%
20%
80%
SWRs with
spatial reactivation
no spatial reactivation
C
***
R² for position decoding
0.5
0.25
0
SUB CA1
D
***
% MF cell per SWR
1
0.8
0.6
0.4
0.2
0
n.s.
SUB
CA1
SWRs with
spatial reactivation
no spatial reactivation

894 **Figure 8. Spatial reactivation in SWR is more prevalent in the CA1 than in the subiculum**

895 **(A)** Example SWRs with spatial reactivations of the subiculum (left panel) and the CA1 (right
896 panel) are shown. In each SWR, the leftmost line plot and raster plot show the LFP changes
897 and single cell firing during the SWR. The middle colormaps show each single cell's on-track
898 firing rate map. The rightmost plot shows the posterior probability of the decoded position
899 during each SWR (see Materials and Methods for detailed description). **(B)** Proportion of
900 SWRs with spatial reactivation in the subiculum and the CA1. **(C)** Comparison of $R^2$ value (the
901 linear regression strength) for the posterior probability of the decoded position during SWRs
902 between the subiculum and CA1. **(D)** Proportional differences of MF cells calculated for each
903 SWR event between SWRs with or without spatial reactivation (data are presented as means ±
904 standard error of the mean). ***$p$<0.001. St box, start box; choice, choice point; fw, food well;
905 SUB, subiculum.

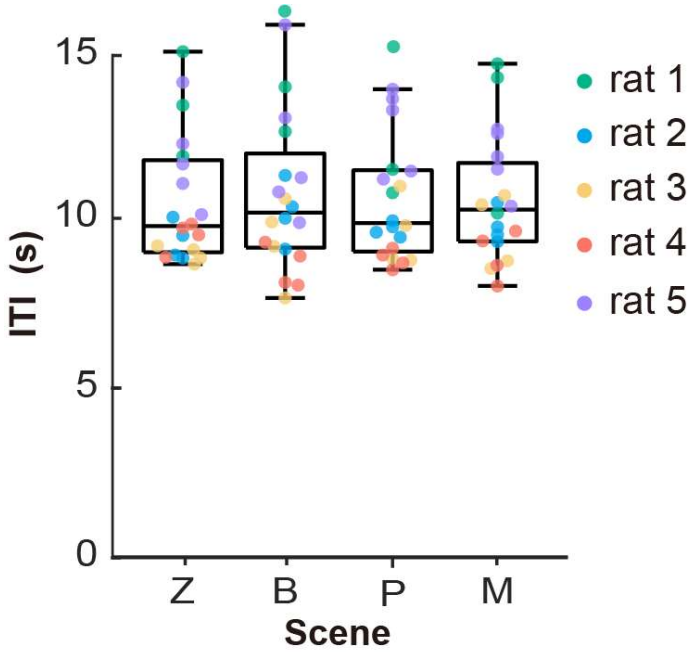


**Figure S1. No difference in ITI duration among visual scenes**

Comparison of ITI durations among trial scene conditions. Box plot indicates median and interquartile values of the ITI duration for all rats in each scene. Each dot indicates the average ITI (excluding ITIs after incorrect trials) for each session, with sessions from the same rat depicted by the same color. Z, Zebra; B, Bamboo; P, Pebbles; M, Mountain

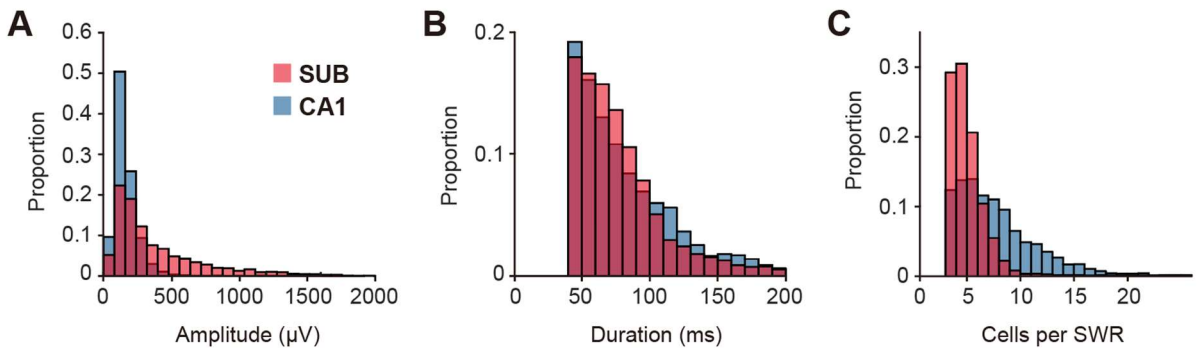


**Figure S2. SWR property difference between the subiculum and CA1**

Comparison of SWR properties between the subiculum and CA1. **(A)** Distribution of average filtered LFP amplitudes during SWRs (150-250Hz). **(B)** Distribution of SWR durations. **(C)** Histogram of the number of activated cells per SWR. SUB, subiculum.

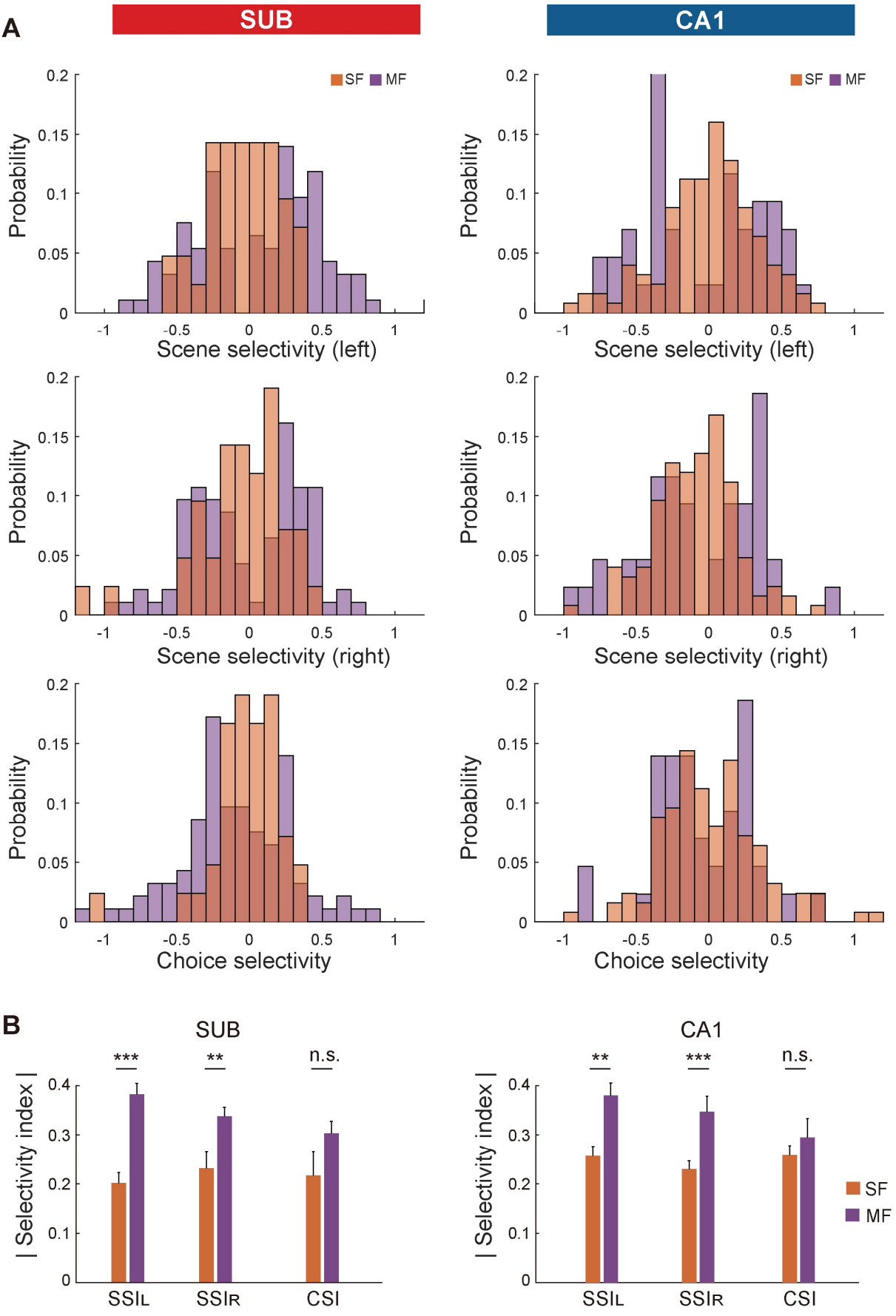
A
SUB
CA1
SF
MF
Probability
Scene selectivity (left)
Scene selectivity (right)
Choice selectivity
B
SUB
CA1
| Selectivity index |
***
**
n.s.
SSIL
SSIR
CSI

917

**Figure S3. Selectivity index distribution of θ-phase-based subfields**

(A) Histograms show selectivity index distribution (for $SSI_L$, $SSI_R$ and CSI in separate plots) of θ-phase-based subfields in the subiculum (left) and the CA1 (right). **(B)** Comparison of the absolute values of selectivity indices between SF and MF cells in the subiculum (left) and CA1 (right). Data are presented as means ± standard error of the mean. *** $p<0.001$. SF, single-field; MF, multi-field.

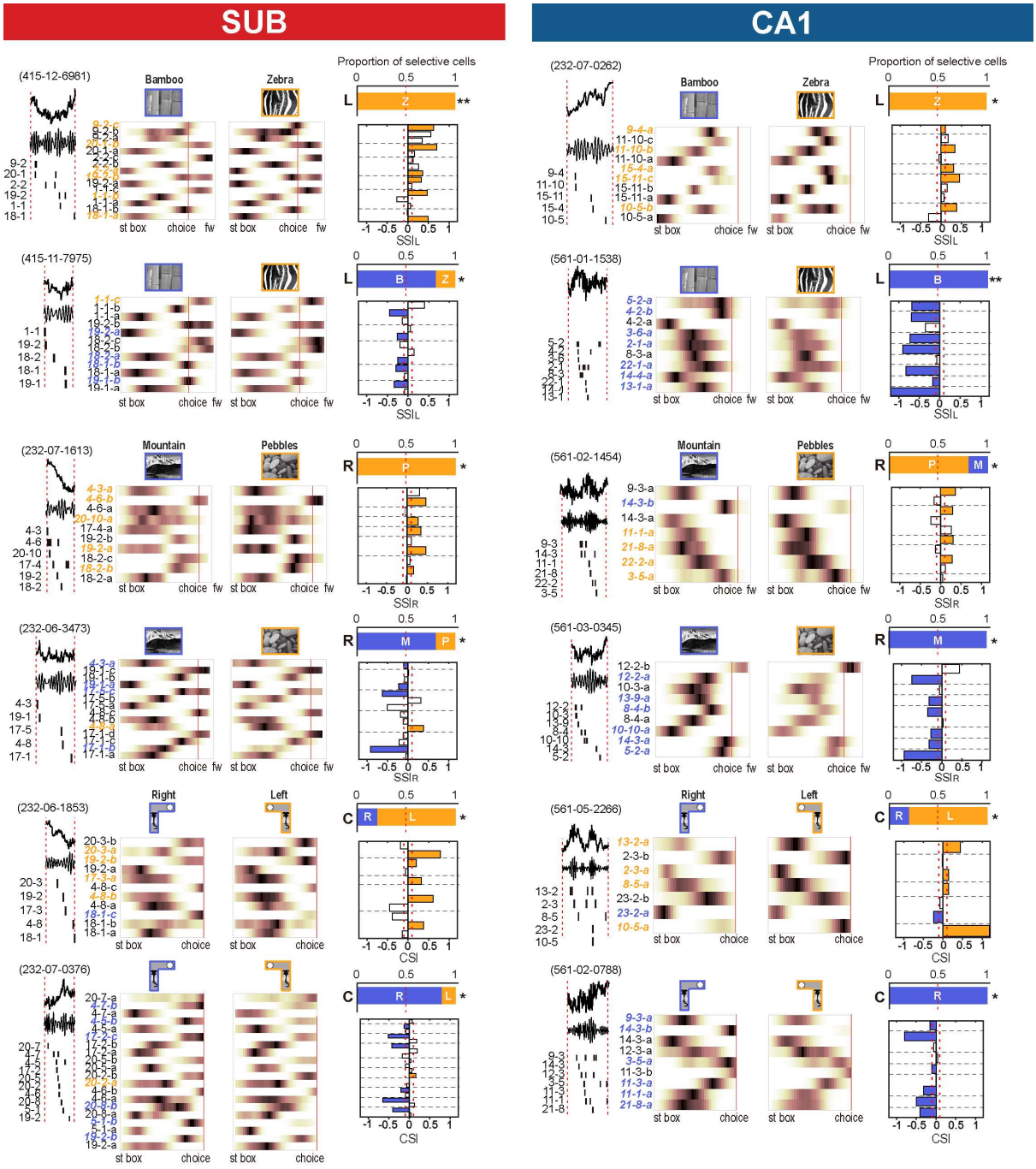
SUB
CA1
Proportion of selective cells
(415-12-6981)
Bamboo
Zebra
(232-07-0262)
(415-11-7975)
(561-01-1538)
(232-07-1613)
Mountain
Pebbles
(561-02-1454)
(232-06-3473)
(561-03-0345)
(232-06-1853)
Right
Left
(561-05-2266)
(232-07-0376)
(561-02-0788)
st box
choice
fw
SSIL
SSIR
CSI

924

**Figure S4**. **Original version of SWR examples in Figure 4, which include all θ-phase-based subfields of reactivated cells**

Example SWRs with TDA reactivations of the subiculum (left) and the CA1 (right). In each example, the leftmost part shows filtered LFP trace and spiking activities of cell ensemble within SWR boundaries. The middle colormaps represent the on-track firing rate map of all θ-phase-based subfields for selected task condition. For the example SWRs with choice reactivation, "arm" sections of T-maze, from choice point to food well, are excluded from display, since those sections are not used to calculate choice selectivity index. The top right graph depicts the proportion of cells in the reactivated ensemble that are selective to certain trial conditions. The statistical significance of ensemble-level selectivity bias calculated by a binomial test is indicated as asterisks. The bottom right bar graphs are selectivity indices for θ-phase-based subfields, color-coded by trial conditions. θ-phase-based subfields in the same cell are indicated by a dotted line.

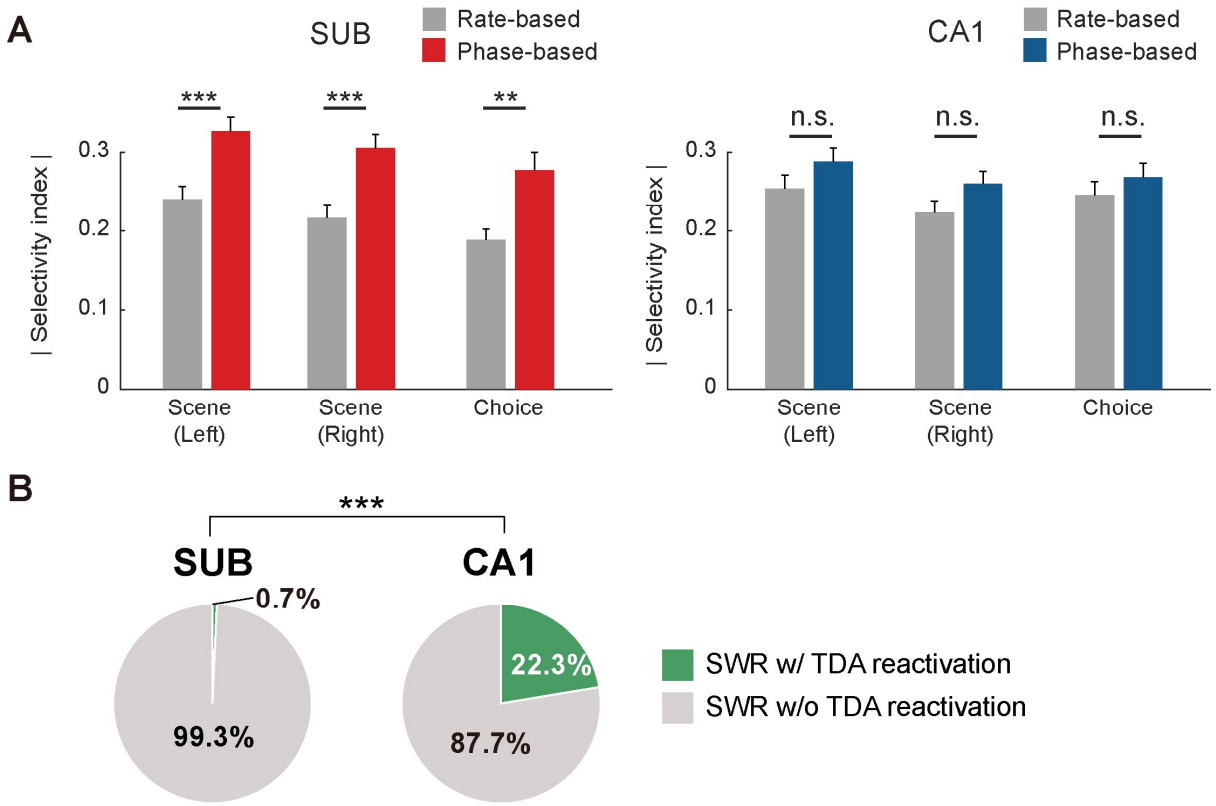


**Figure S5. Reduced occurrence of TDA reactivation after firing rate-based field identification**

**(A)** Bar graphs comparing the absolute values of the selectivity index calculated from rate-based field versus θ-phase-based field in the subiculum (left) and CA1 (right). In each region, the selectivity index is compared for the left-choice scene pair (zebra-bamboo), the right-choice scene pair (pebbles-mountain), and the choice pair. Data are presented as means ± standard error of the mean. **(B)** Proportion of TDA reactivations among all SWRs in the subiculum and the CA1, when the selectivity index of each cell is calculated from the rate-based field. $^{**}p<0.01$, $^{***}p<0.001$. SUB, subiculum.

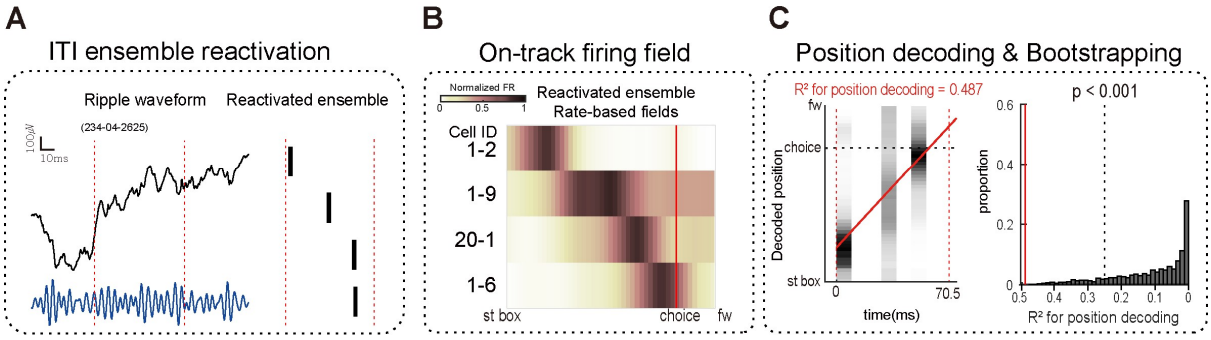


**Figure S6. Detection process of spatial reactivation**

**(A)** An example SWR during inter-trial interval is shown (in the same manner as Figure 3A). **(B)** On-track firing rate maps for each cell on the track. Each cell in a row is the cell in the same relative row in the raster plot of (A). The numbers on the left side of each row indicate the cell ID. Firing rates in each map are normalized by the cell's maximum firing rate (color bar at the upper left). **(C)** The posterior probability of the decoded position during the SWR is shown on the left panel. A red dashed line represents the linear regression line. The $R^2$ value of the line is at the top of the graph. Bootstrap process to calculate the significance of the regression line for the decoded position is shown on the right panel. The red line indicates the position of the example SWR's $R^2$ value from the distribution. The p-value represents the proportion of random distribution values larger than the example SWR's $R^2$ value.